INTERNATIONAL ATOMIC ENERGY AGENCY
UNITED NATIONS EDUCATIONAL, SCIENTIFIC AND CULTURAL ORGANIZATION
INTERNATIONAL CENTRE FOR THEORETICAL PHYSICS
I.C.T.P., P.O. BOX 586, 34100 TRIESTE, ITALY, CABLE CENTRATOM TRIESTE

H4-SMR 393/50

SPRING COLLEGE ON PLASMA PHYSICS

15 May - 9 June 1989

ANOMALOUS TRANSPORT AND FLUCTUATIONS IN PLASMAS

A. J. Wootton

Fusion Research Center
University of Texas at Austin
Austin
U. S. A.

ANOMALOUS TRANSPORT AND FLUCTUATIONS IN PLASMAS

(A series of 3 lectures)

A. J. Wootton

Fusion Research Center
University of Texas at Austin
Austin
Tx 78712
USA

Lecture 1 Diagnostic and Analysis Techniques

Abstract

This first lecture is intended to provide the motivation for studying fluctuations in plasmas, and how we go about measuring them. I start by describing the many problems which present day neoclassical theory has in explaining tokamak plasma transport. The possible importance of plasma fluctuations and turbulence is then introduced, and the parameters necessary to identically determine any fluctuation driven fluxes, for comparison with total fluxes, are described. In general not all of these parameters can be measured, and possible strategies for overcoming the limitations of incomplete data are presented. This section is followed by a description of some of the more important diagnostics which are commonly used to determine fluctuations: in particular Langmuir probes, induction coils, wave scattering techniques, and the heavy ion beam probe. The advantages and limitations of each diagnostic are made clear. Various statistical techniques which allow useful quantities to be extracted from time series data are introduced.

Lastly, an experimentalists interpretation of some of the theoretical models proposed to explain turbulent transport is presented.

Contents:

TRIESTE AJW/FRC 4/26/89

Lecture 2 Electrostatic Turbulence in Tokamaks

Abstract

In the second of three lectures, I discuss the application of the ideas outlined in lecture 1 to electrostatic fluctuations in tokamak plasmas. In particular, the plasma edge is particularly suitable to study by material probes, and it is possible to measure all the quantities necessary to determine the electrostatic fluctuation driven particle and electron heat fluxes. The microscopic properties of the fluctuations, such as fluctuation levels and phase velocity, are first discussed. Then the fluctuation driven fluxes are compared with the total fluxes, as found from power balance or the response of the plasma to transients. It is shown that the measured electrostatic fluctuations play an important role in both particle and energy escape across the plasma edge. However, no suitable model exists to describe what we measure.

In the plasma interior the problem of comparing fluctuation driven fluxes with total fluxes is more difficult, both because of the lack of data and the many different (poloidally asymmetric) phenomena which occur. After describing the general characteristics of the interior turbulence, an attempt is made to compare the predictions of various theoretical models with the measured total fluxes, using where possible experimentally measured turbulence characteristics. I conclude that we cannot yet show an unambiguous relationship between interior fluctuations and transport, as we could at the edge.

Contents:

Lecture 3 Magnetic turbulence in tokamaks

Abstract

In this last lecture, I address what is known about magnetic turbulence in tokamaks, and its effects on transport. Three sections are presented: on coherent modes, incoherent modes (turbulence), and externally generated magnetic perturbations. Coherent modes are thought to lead major transport changes, such as sawteeth oscillations, and plasma disruptions. The incoherent, or turbulent, fluctuations are thought by many to be responsible for plasma energy transport, especially at high plasma pressure. The conflicting and incomplete evidence relating magnetic turbulence and plasma transport is presented.

Lastly, the effects of extrinsic magnetic turbulence, generated by currents flowing in coils outside the plasma, is discussed. Both magnetic islands and stochastic regions can be generated, and have been proposed for particle and energy control schemes. We show that, while the heat fluxes can be well explained by test particle theories, the particle flux is unexplained.

Contents:

DIAGNOSTIC AND ANALYSIS TECHNIQUES

Contents:

1.1 TOKAMAK TRANSPORT

How to measure the total fluxes, and a comparison of total fluxes with neoclassical predictions

Working particle flux Γ^i:

$$\Gamma^i = -D^i\nabla n + nv^i$$

Γ^i is determined experimentally from spectroscopic measurements of the particle source S (using H_α light emission) by invoking continuity:

$$dn/dt = -\nabla\cdot\Gamma^i + S$$

Plasma edge: behind a limiter, parallel and perpendicular flow can be balanced to derive a radial diffusion coefficient $D^i \approx 1m^2s^{-1}$.

Plasma interior: the coefficients D^i and v^i are separately determined by following the time response of the density profile to a perturbation, e.g.

an oscillating gas feed,

density sawteeth,

a pellet of solid fuel.

$D^i \approx 1m^2s^{-1}$ $(D^{i,nc} \approx 1x10^{-3}m^2s^{-1})$

$v^i \approx 10ms^{-1}$ $(v^{i,nc} \approx 1ms^{-1})$.

There are some reported cases, near the plasma axis, where v^{nc} is in agreement with the experimental values.

Impurity particle flux Γ^z:

$$\Gamma^z = -D^z\nabla n + nv^z$$

D^z and v^z determined, like the working gas, from following time dependent perturbations.

$$D^z \approx D^i \approx 1m^2s^{-1} \approx 10D^{z,nc}$$

$$v^z \approx v^{z,nc} \approx 10ms^{-1}.$$

The scalings of D^z and D^i with global plasma parameters are not the same. However, the technique used for impurities results in an intrinsic spatial weighting of v^z towards the plasma edge, and of D^z towards the plasma center.

Certain characteristic features of impurity behavior <u>are</u> predicted by neoclassical theory, e.g.

impurity accumulation with co-neutral beam injection or pellet injection without sawteeth,

impurity expulsion with counter neutral beam injection or asymmetric working gas feed.

Momentum diffusivity

is determined by following the response of the plasma rotation velocity to a momentum source.

The results are generally interpreted in terms of an anomalous viscosity, although a neoclassical gyroviscous model has been proposed to explain the results. This mechanism does not explain rotation results from TFTR.

Thermal fluxes (q) and diffusivities (χ)

are determined from an analysis of the radial profiles of input power, electron temperature T_e, ion temperature T_i, density n, radiation P_{rad}, charge exchange loss P_{cx}, and particle source S. The electron heat flux deduced (as a remainder) is always anomalously high, being typically 10^2 to 10^3 times the neoclassical prediction.

Propagation of locally produced heat pulses gives a value a few times that derived from the profile analysis (sawteeth, ECRH, Alfven waves).

Ion thermal fluxes are closer to the neoclassical predictions, but as more detailed information on $T_i(r)$ is becoming available, the ion thermal diffusivity χ_i can be >10 times χ_i^{nc}, with $\chi_i \approx \chi_e \approx 4D^i$.

1.2. THE ROLE OF FLUCTUATIONS

What we should measure, what we can measure

Neoclassical predictions assume that the density n, electric field E, temperature T, magnetic field b and current density j are stationary. Let the respective fluctuating quantities be represented by $\tilde{n}$, $\tilde{E}$, $\tilde{T}$ and $\tilde{j}$ respectively. Ignoring poloidal and toroidal asymmetries, and assuming $\omega \ll \omega_{ci}$, the ion cyclotron frequency, then the fluctuation driven radial fluxes (denoted by superscript f) for each species (subscript j) are given by electrostatic (superscript E) and magnetic (superscript b) terms:

Particle flux $\Gamma^f_j = \Gamma^{f,E_j} + \Gamma^{f,b_j}$

$$\Gamma^{f,E_j} = \langle \tilde{E}_\theta \tilde{n}_j \rangle / B_\phi$$

$$\Gamma^{f,b_j} = -\langle \tilde{j}_\parallel \tilde{b}_r \rangle / (eB_\phi) = g1(\tilde{b}_r/B_\phi)$$

Energy flux $Q^f_j = Q^{f,E_j} + Q^{f,b_j}$

$$Q^{f,E_j} = 3/2\ k_b\ n \langle \tilde{E}_\theta \tilde{T}_j \rangle / B_\phi + 3/2\ k_b\ T_j \langle \tilde{E}_\theta \tilde{n}_j \rangle / B_\phi$$

$$Q^{f,b_j} = g2(\tilde{b}_r/B_\phi)$$

The exact form for the functions $g1(\tilde{b}_r/B_\phi)$ and $g2(\tilde{b}_r/B_\phi)$ depend on the exact plasma parameters, but typically $g1(\tilde{b}_r/B_\phi)$ is negligible and $g2$ is taken as the quasi linear expression:

$$g2(\tilde{b}_r/B_\phi) \approx \pi R\, v_{the}\, (\tilde{b}_r/B_\phi)^2 \quad \text{collisionless plasma}$$

$$g2(\tilde{b}_r/B_\phi) \approx \chi_{e\|}(\tilde{b}_r/B_\phi)^2 \quad \text{collisional plasma}$$

In strong turbulence (superscript ST) regimes the collisionless expression is modified to :

$$g2^{ST}(\tilde{b}_r/B_\phi) \approx \delta_\perp\, v_{the}\, ((\tilde{b}_r/B_\phi)^2)^{1/2} \quad \text{collisionless}$$

with

$$\delta_\perp = k_\perp^{-1}, \text{ a perpendicular wavelength.}$$

It is customary to split the energy flux Q into a conducted heat flux q and the convected flux $5/2\, k_b T_j \Gamma_j$:

$$Q_j = q_j + 5/2\, k_b T_j \Gamma_j$$

so that

$$q_j = 3/2\, k_b\, n \langle \tilde{E}_\theta \tilde{T}_j \rangle / B_\phi + f((\tilde{b}_r/B_\phi)) - k_b T_j \Gamma_j$$

There is disagreement in the literature as to whether the factor in the electrostatic component of the energy flux is 3 or 5: the difference is related to the contribution made by the turbulence to the energy source $\langle \tilde{E}.\tilde{j} \rangle$ Theoretical models usually provide Q, independent of the choice of constants.

Results from TFTR suggest that the convected energy flux is $3/2\, k_b T_j \Gamma_j$, rather than $5/2\, k_b T_j \Gamma_j$; i.e. a factor 3/2 should be used.

In the plasma edge.

If we could measure $\tilde{n}$, $\tilde{E}$, $\tilde{T}$ and their correlations throughout the plasma volume, we could identically measure the electrostatic components of the various fluctuation driven fluxes. We can do this **at the plasma edge** using probes.

For example, the electrostatic particle flux $\Gamma^{f,E}$, and therefore the convected part of the energy flux, is measured as a function of frequency $\omega/2\pi$ in terms of the root mean square (rms) fluctuation levels:

$$\Gamma^{f,E}(\omega,k) = \tilde{n}_{rms}\, \tilde{\phi}_{rms}\, |\gamma_{n\phi}|\, k_\theta(\omega)\, \sin(\alpha_{n\phi}(\omega))/B_\phi$$

where k is the measured wave number, $\tilde{\phi}$ is the measured fluctuating plasma potential ($=\tilde{E}_\theta/k_\theta$), $\gamma_{n\phi}$ is the measured coherence between $\tilde{n}$ and $\tilde{\phi}$, and $\alpha_{n\phi}$ the measured phase between $\tilde{n}$ and $\tilde{\phi}$.

To determine the electrostatic energy flux $Q^{f,E}$ we need the correlation between $\tilde{E}$ (or $\tilde{\phi}$) and $\tilde{T}$, which is not generally known. However, an upper bound can always be placed by assuming perfect correlation (i.e. $\gamma_{T\phi}=1$, $\sin(\alpha_{T\phi})=1$).

To estimate the magnetic components $\Gamma^{f,b}$ and $Q^{f,b}$ we should measure $\tilde{j}_\|$ and $\tilde{q}_\|$, but this is not done. Instead $\tilde{b}$ is measured, and then models applied to derive the fluxes.

In the plasma confinement region

The diagnostic problem is more difficult, because the high parallel heat flux precludes the use of material probes.

Scattering of microwaves or laser light, together with Fast Fourier Transform [FFT] spectral analysis, is commonly used to determine the spectral power density distribution function $S(k,\omega)$, where

$$\langle |\tilde{n}|^2 \rangle = (2\pi)^{-4} \int dk^3 d\omega S(k,\omega)$$

The heavy ion beam probe (HIBP) allows simultaneous measurements of both density and potential fluctuations summed over a large range of k, $0<k_\perp<5mm^{-1}$, together with $\alpha_{n\phi}$ and $\gamma_{n\phi}$ for $0<k_\perp<0.5mm^{-1}$.

No diagnostics yet exist which give relevant information on $\tilde{T}$ in the confinement region, and except on small, low temperature machines the only information on $\tilde{b}$ is inferred from runaway electron confinement properties.

Therefore in the plasma interior of large machines we are restricted to directly measuring only $\Gamma^{f,E}$, with the HIBP.

It seems unlikely that we shall be able to measure the correlations necessary to determine identically the internal fluctuation driven fluxes in the near future (i.e. α_{ET}, γ_{ET}).

Therefore information on $\Gamma^{f,b}$, $q^{f,E}$ and $q^{f,b}$ must come as now from using what we can measure (e.g. $\tilde{n}(k,\omega)$ and $\tilde{\phi}(k,\omega)$) in various models.

In the future $\tilde{T}_e$ may become available from electron cyclotron emission (ECE) measurements, and $\tilde{b}$ from HIBP measurements.

Having measured interior fluctuating amplitudes, it is natural to seek correlations between this amplitude and plasma transport coefficients. However, one should not necessarily expect to find a direct correlation, because:

1) the problem of possible geometric asymmetries, addressed later: neither a point nor line of sight measurement of a fluctuating quantity is adequate.

2) the choice of applicable turbulence regime (flux $\alpha (\tilde{n}/n)^2$, $(\tilde{n}/n)^1$ or $(\tilde{n}/n)^0$ in quasi linear, strong turbulence, and stochastic regimes has been proposed). However, we should be able to distinguish which is the applicable regime from the measurements of the turbulence microstructure itself.

3) other varying plasma parameters (such as T_e) appear in the relationship between a flux or transport coefficient and a fluctuation level.

e.g. for drift waves

$$q_e = n_e T_e \left(\frac{c T_e}{e B_\phi}\right) \sum_{k_\theta} \left[k_\theta \left(\frac{\tilde{n}}{n}\right)^2 \xi(k)\right]$$

$$\xi(k) = \frac{4}{\pi^{1/2}} \epsilon^{3/2} \frac{\omega_*}{\nu_e} \left[\frac{k_\perp^2 \rho_s^2}{1 + k_\perp^2 \rho_s^2} + \frac{3}{2}\eta_e\right]$$

$$\omega_* = \frac{k_\theta T_e}{n_i e B_\phi} \, dn/dr$$

$$\eta_e = \frac{L_n}{L_{T_e}}$$

i.e. $q_e \neq \text{const.} \times \left(\frac{\tilde{n}}{n}\right)^2$!

1.3 DIAGNOSTICS

LANGMUIR PROBE

Case 1

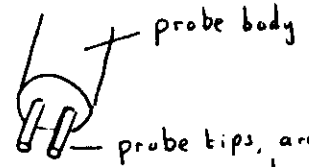

2 pin probe, aligned $\perp$ to B

$$I = a A n_e \sqrt{\frac{2T_e}{m_i}} \tanh\left(\frac{eV - V_d}{2T_e}\right)$$

V is applied
V_d is floating pot. diff.

Taylor expand, normalise ($\tilde{\imath} \Rightarrow \tilde{\imath}/I$; $\tilde{n} \Rightarrow \tilde{n}/n$; $\tilde{T} \Rightarrow \tilde{T}_e/T_e$;
$\tilde{V}_d \Rightarrow \tilde{V}_d/kT_e$; $x = eV/kT_e$)

$$\tilde{\imath} = f_1^2 \tilde{n}^2 + f_2^2 \tilde{T}_e^2 + f_3^2 \tilde{V}_d^2 + 2 f_1 f_2 \langle \tilde{n} \tilde{T} \rangle + 2 f_1 f_3 \langle \tilde{n} \tilde{V}_d \rangle + 2 f_2 f_3 \langle \tilde{T} \tilde{V}_d \rangle$$

where $f_1 = \tanh(x/2)$
$f_2 = \frac{1}{2}\tanh(x/2) - x\,\mathrm{sech}^2(x/2)$
$f_3 = -\frac{1}{2}\mathrm{sech}^2(x/2)$

} all known functions of the applied voltage V

and $V_d = E_\theta d$

So plot $\tilde{\imath}$ against V, Fit expression, determine the coefficients $\tilde{n}^2$, $\tilde{T}_e^2$, $\tilde{V}_d^2$, $\langle \tilde{n} \tilde{T} \rangle$, $\langle \tilde{n} \tilde{V}_d \rangle$, $\langle \tilde{T} \tilde{V}_d \rangle$

Fig.2a

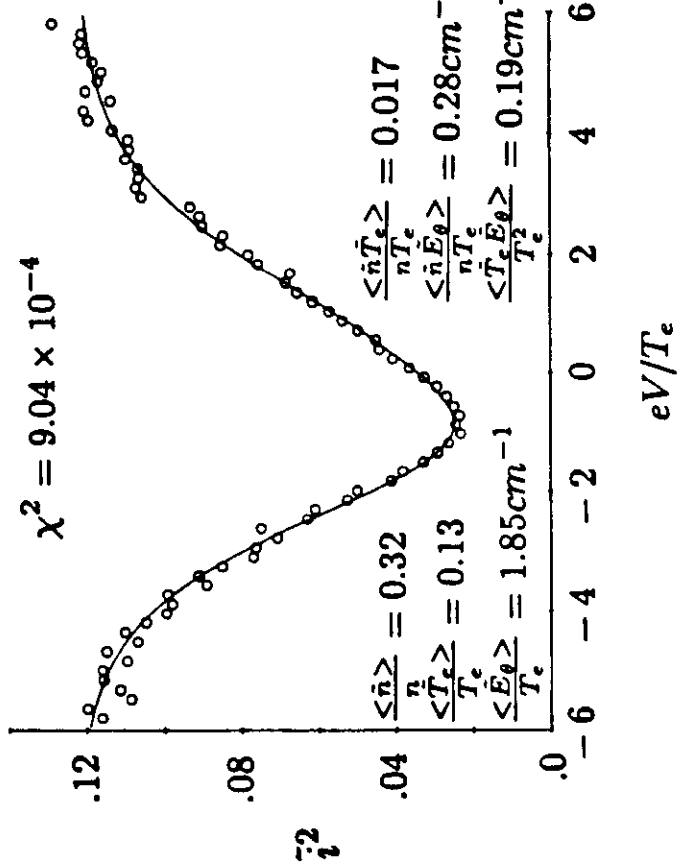

LANGMUIR PROBE

Case 2

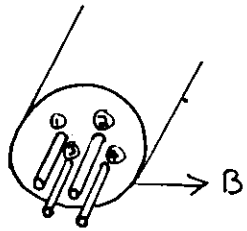

4 pin probe

pins 1 & 2 biased ~200V, measure I_{sat}

probes 3 & 4 : floating

$T_e(t) = k(\phi_1 - \phi_2)$

$k_\Theta(t) = \Theta_{3,4}/d$

$\phi_p(t) = \phi_4(t) + 3.1\, k T_e(t)$

$n_e(t) = I_{sat}/\sqrt{T_e}$

$\Rightarrow$ steady state n, T profiles, as well as everything we need to compute $\Gamma^{T.E}$ and convected energy flux

eg $\Gamma = \frac{1}{B} \left\langle \frac{\tilde{n}\,\tilde{\phi}}{d} \right\rangle$ as $f(t)$

- but no ω, k information this way
- must have $d \ll 1/k$

INDUCTION COIL

$V = nA\,\dot{B}$

- Multiple arrays used, typically at the vacuum vessel, allows m, n values to be determined.
- If we know $q(r)$, then we can Fourier analyze $\tilde{b}$ at the vessel for all $m/n = q$, and extrapolate in to find $\tilde{b}(r)$.
- The extrapolation is good as long as there is no shielding
- The decay of $\tilde{b}$ outside the plasma is also used to determine m.

WAVE SCATTERING

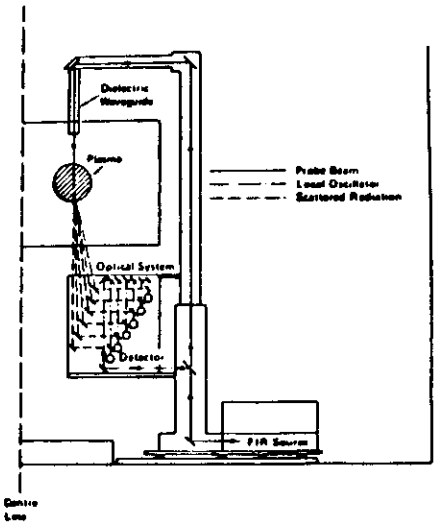

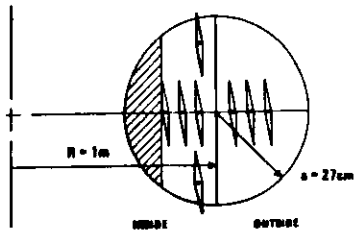

(for $k_\perp = 12 cm^{-1}$)

Fluctuations with $\omega,\mathbf{k}$

Scattered wave with $\omega_S,\mathbf{k}_S$ } $\omega_S = \omega_0 \pm \omega$, $\mathbf{k}_S = \mathbf{k}_0 \pm \mathbf{k}$

Input wave with $\omega_0,\mathbf{k}_0$

For $\mathbf{k}$'s of interest $\mathbf{k}_S \approx \mathbf{k}_0$, and $k = 2k_0 \sin(\theta_S/2)$.

Typically $\lambda_0 = 2\pi/k_0 \approx 10^3 \mu m$ (FIR)

Mix local oscillator and scattered signal beams in the receiver. This provides an output proportional to the electric field E of the scattered radiation. The scattered power α S(**k**), the spectral density function:

$$|\langle\tilde{n}\rangle|^2 = \int S(\mathbf{k})d\mathbf{k}/(2\pi^3)$$

HETERODYNE DETECTION: The FIR source is a twin frequency laser, producing $\omega_0 \approx 245$GHz and $\omega_0 + \Delta\omega$, with $\Delta\omega \approx 1$MHz. The frequency shifted scattered beam and local oscillator mix in a Schottky diode receiver, to give a signal $\alpha \cos((\Delta\omega \pm \omega)t)$. If $\Delta\omega >> \omega$, the propagation direction is resolved as two sidebands $\pm\omega$ about ω.

HOMODYNE DETECTION: The FIR source is a single ω, divided into a local oscillator and probe beam. The detected signal $\alpha \cos(\pm\omega t)$

From these measurement we can determine the frequency integrated spectral density function

$$S(k) \alpha \tilde{n}(k)^2,$$

the wave number integrated spectral density function

$$S(\omega) \alpha \tilde{n}(\omega)^2,$$

and various spectral averages

e.g. $$\overline{v_{ph}} = \Sigma_{\omega,k}(\omega/k)S(k,\omega)/\Sigma_{\omega,k}S(k,\omega),$$

$$\overline{k} = \Sigma_{\omega,k}kS(k,\omega)/\Sigma_{\omega,k}S(k,\omega)$$

Typically $0<k_\perp<1.5mm^{-1}$ (where $\mathbf{k}_\perp = \mathbf{k}_r + \mathbf{k}_\theta$). With heterodyne detection the electron drift direction and ion drift direction spectral density functions (S_e and S_i) can be separated. A significant advantage of wave scattering is that **k** is well defined. However, line of sight measurements (subscript los), with little spatial resolution, are often used.

HEAVY ION BEAM PROBE

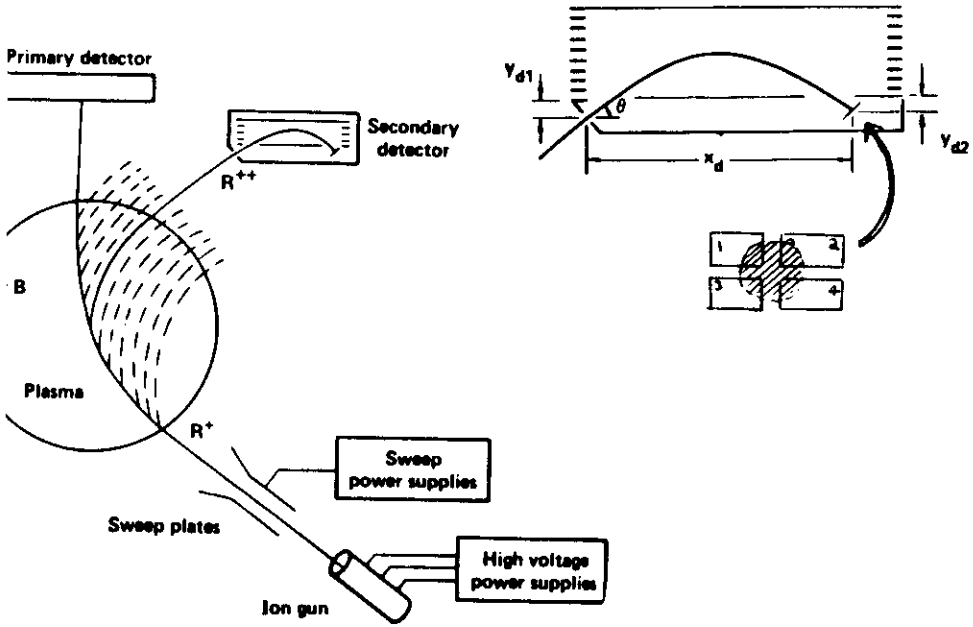

Sample volume position specified by geometry, B_ϕ, E^+.

Measure secondary current to each of 4 detectors, and compute:

$I_{sum} = I_1 + I_2 + I_3 + I_4$: info on $\tilde{n}/n$

$I_{up/down} = (I_1 + I_2) - (I_3 + I_4)$ info on $\tilde{\phi}$

$I_{left-right} = (I_1 + I_3) - (I_2 + I_4)$ info on $\tilde{b}$

$\tilde{n}/n$:

$$I_{sum} = I_0 + \exp(-\int n_e \langle\sigma v\rangle^{1\text{-}2} dl_{in})\ (n_e \langle\sigma v\rangle^{1\text{-}2})_{sv}\ \exp(-\int n_e \langle\sigma v\rangle^{2\text{-}3} dl_{out})$$

input beam attenuation	ionization in sample volume	output beam attenuation

$T_e > 100$ev, small radial correlation length: $\tilde{I}_{sum}/I_{sum} = \tilde{n}/n$

$\tilde{\phi}$: note the up/down position in the analyzer gives the kinetic energy of the secondary beam.

$$E_{out} = E_{in} + (q_{out}-q_{in})e\phi = E_{in} - e\phi$$

$$\tilde{I}_{up/down}\ \alpha\ \tilde{E}_{out} = e\tilde{\phi}$$

---

k_θ: Use two sample volumes displaced by Δx (in the poloidal direction). Measure the phase angle $\theta(\omega)$:

$$k = \theta/\Delta x$$

$\tilde{b}$: toroidal displacements ($I_{left-right}$) are produced by b_r,b_θ along the line of sight.

Examples of single point HIBP data

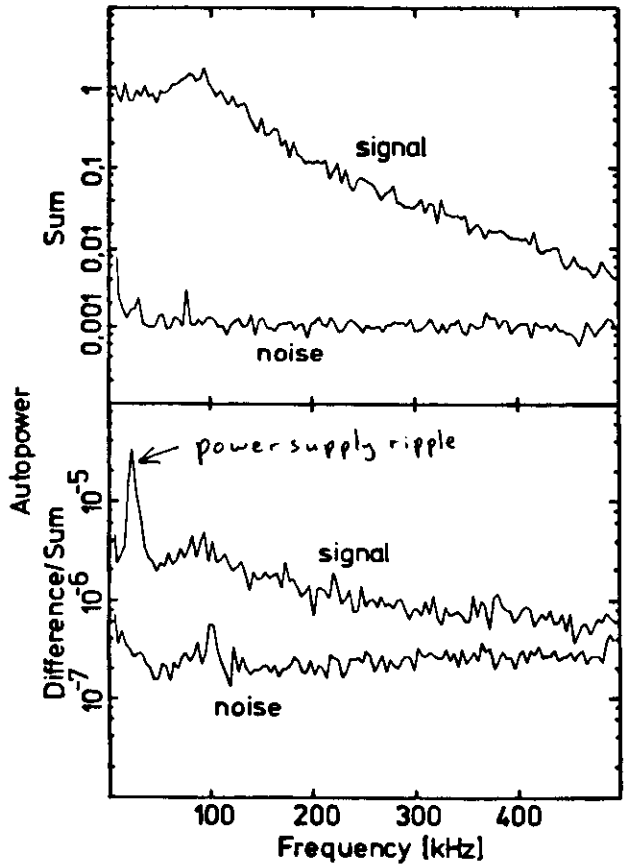

Sum and Difference Noise Levels

20a)

Example of HIBP 2 point data.

2 points separated by 1.5cm

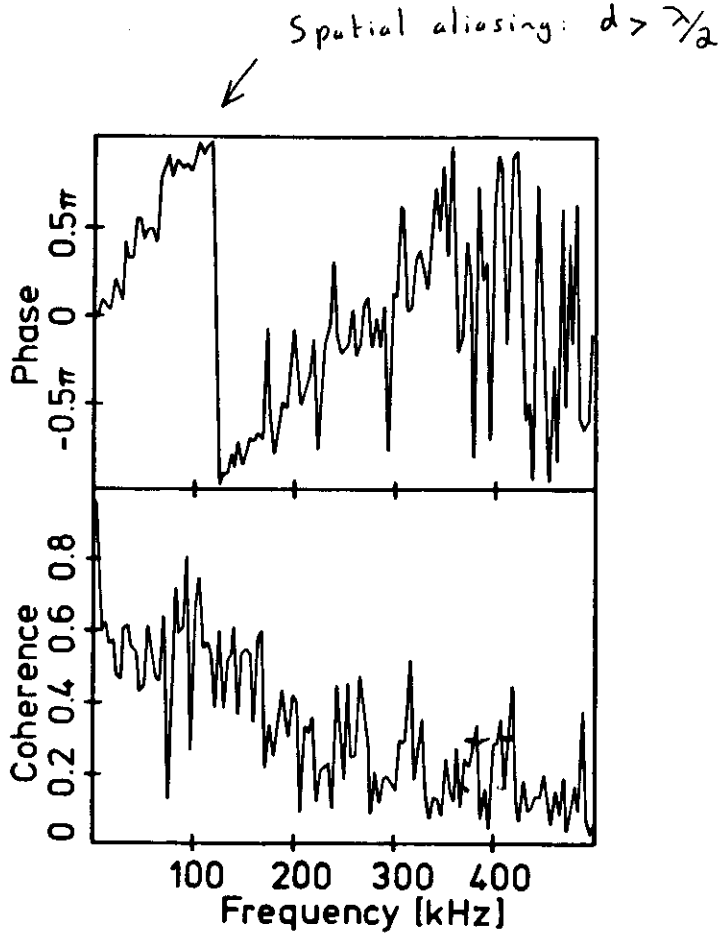

Two Point Coherence and Phase Shift

20b)

1.4 DATA ANALYSIS TECHNIQUES

a) Linear (HIBP, LP)

Scattering techniques measure the k spectrum directly. Both the HIBP and Langmuir probes utilize a two point correlation technique. This adaption of the linear FFT spectral analysis allows fluctuation driven fluxes to be deduced.

$$\langle \tilde{n}\tilde{v} \rangle = 1/B.\ \langle \tilde{n}\tilde{E} \rangle = 1/B.C_{nE}(0)$$

$C_{nE}(0)$ is the cross correlation function $C_{nE}(\tau)$ between density and electric field fluctuations evaluated for $\tau = 0$:

$C_{nE}(\tau)$ may be expressed as the Fourier transform $P_{nE}(\omega)$ of the cross power spectrum:

$$C_{nE}(\tau) = \langle \tilde{n}(t)\ \tilde{E}(t+\tau) \rangle = \int_{-\infty}^{\infty} P_{nE}(\omega)\exp(-i\omega\tau)d\omega$$

Symmetry (absolute value even, phase odd function of ω):

$$C_{nE}(\tau) = \langle \tilde{n}(t)\ \tilde{E}(t+\tau) \rangle = 2\ \mathrm{Re}\int_{0}^{\infty} P_{nE}(\omega)\exp(-i\omega\tau)d\omega, \text{ and}$$

$$\langle \tilde{n}\tilde{v} \rangle = 2/B.\mathrm{Re}\int_{0}^{\infty} P_{nE(\omega)}d\omega \ = -2\ /B.\mathrm{Re}\int_{0}^{\infty} ik(\omega)P_{n\phi}(\omega)d\omega$$

with $k(\omega) = \theta/\Delta x$

INTERPRETATION

Use $P_{n\phi}(\omega) = |P_{n\phi}(\omega)|\ \exp(i\alpha_{n\phi}(\omega))$:

$$\langle \tilde{n}\tilde{v} \rangle = 2/B\int_{0}^{\infty} k(\omega)|P_{n\phi}(\omega)|\ \sin[\alpha_{n\phi}(\omega)]d\omega$$

Multiply and divide by $[P_{nn}(\omega)P_{\phi\phi}(\omega)]^{1/2}$, and use

$$\tilde{n}_{rms} = (2P_{nn}(\omega)d\omega)^{1/2}$$

$$\tilde{\phi}_{rms} = (2P_{\phi\phi}(\omega)d\omega)^{1/2}$$

$$|\gamma_{n\phi}(\omega)| = |P_{n\phi}(\omega)|/[P_{nn}(\omega)P_{\phi\phi}(\omega)]^{1/2}$$

Then:

$$\langle \tilde{n}\tilde{v} \rangle_{d\omega} = k(\omega)/B.|\gamma_{n\phi}(\omega)|\ \sin[\alpha_{n\phi}(\omega)]\tilde{n}_{rms}\ \tilde{\phi}_{rms}$$

The above technique suffers serious limitations in the interpretation of average quantities (e.g. $\bar{k}$, $\bar{v}_{ph}$) if two distinct turbulence features coexist. Only the total $\tilde{n}/n$ is measured, not $\tilde{n}/n$ from each turbulence feature separately. Thus counter propagating features such as a coexisting electron and ion feature cannot be separated, and microscopic details of each individual feature cannot be isolated for comparison with theoretical expectations.

PROCESSING 2 POINT DATA

Phase shift derived from phase of cross spectrum.

Raw k estimates used to construct an (ω,k) spectrum similar to a histogram.

The ω,k spectrum S(k,ω) is divided into a number of cells.

The size of each cell in frequency is given naturally by N/(MT), with N the no of samples from each point, T the data duration, and M the amount of averaging in the processing.

The size of each cell in k is somewhat arbitrary. The time series from the points are broken into M segments, and the raw k computed for each segment. The power of each segment is then placed in the appropriate cell of the S(k,ω) histogram.

TRIESTE AJW/FRC 4/26/89

b) Non-linear

(Non linear coupling and 3-wave interactions)

Coupling coefficients and growth rates are basic turbulence characteristics.

Depending on the assumptions and truncations made in deriving the wave eqn., the coefficients vary considerably.

The coupling coefficients, growth rate and dispersion define the spectral shape, which is conserved by a balance of dissipation, linear growth and spectral redistribution.

The wave eqn. for the Fourier spectrum $\phi(k,t)$, where

$\varphi(x,t) = \Sigma\phi(k,t)\exp(ikx)$ is assumed to be:

$$\partial\phi(k,t)/\partial t = [\gamma_k + i\omega_k]\phi(k,t) + 0.5\Sigma\Lambda_k^{Q}{}_{\substack{k_1,k_2 \\ k=k_1+k_2}}(k_1,k_2)\phi(k_1,t)\phi(k_2,t)$$

Represent time derivatives by a difference scheme. The change in the spectrum between t (input) and $t+\tau$ (output) can then be related to the turbulent properties, as long as $\tau \rightarrow 0$ and $\tau << \tau_{\text{wave packet}}$. Writing

$\phi(k,t) = |\phi(k,t)|\exp(i\theta(k,t))$ we can obtain:

$$\phi(k,t+\tau) = L_k\,\phi(k,t) + 0.5\sum_{\substack{k_1,k_2 \\ k=k_1+k_2}} Q_k^{k_1,k_2}\,\phi(k_1,t)\phi(k_2,t)$$

LINEAR QUADRATIC

SO WHAT?

1) Multiply by $\phi^*(k,t)$ and <...>

2) Multiply by $\phi^*(k_{1'},t)\phi^*(k_{2'},t)$ and <...>, with

$k = k_1 + k_2 = k_{1'} + k_{2'}$

Gives two eqns. which can be solved iteratively for L_k and $Q_k^{k_1 k_2}$, and hence γ and L_k, in terms of the statistical quantities:

$< \phi(k,t)\ \phi^*(k,t)>$ auto power spectrum

$< \phi(k,t+\tau)\ \phi^*(k,t)>$ cross power spectrum

$< \phi(k=k_1+k_2,t)\ \phi^*(k_1,t)\phi^*(k_2,t)>$ auto bispectrum

$< \phi(k=k_1+k_2,t+\tau)\ \phi^*(k_1,t)\phi^*(k_2,t)>$ cross bispectrum

All the above can be estimated by ensemble averaging over many independent realizations.

The **POWER TRANSFER** can also be derived from the wave coupling equation by multiplying by $\phi^*(k,t)$, and noting that

$$\partial/\partial t[\phi^*(k,t)] = \phi^*(k,t).\partial\phi(k,t)/\partial t + \phi(k,t)\partial\phi^*(k,t)/\partial t$$

The eqn. for the spectral power $P_k = <\phi(k,t)\phi^*(k,t)>$ is:

$$\partial P_k/\partial t = 2\gamma_k P_k + \mathrm{Re}[\overset{\circ}{\Lambda}_k\ (k_1,k_2)<\phi^*_k\phi_{k1}\phi_{k2}>]$$

i.e. the time change of the spectral power of a wave number is due to the growthand the sum over all components of the power transfer function.

Example of Non-Linear Output

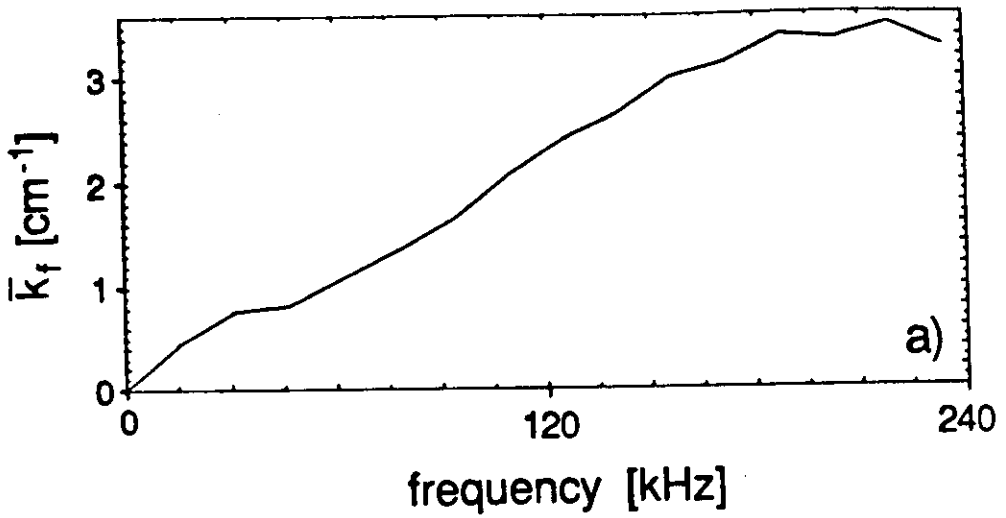

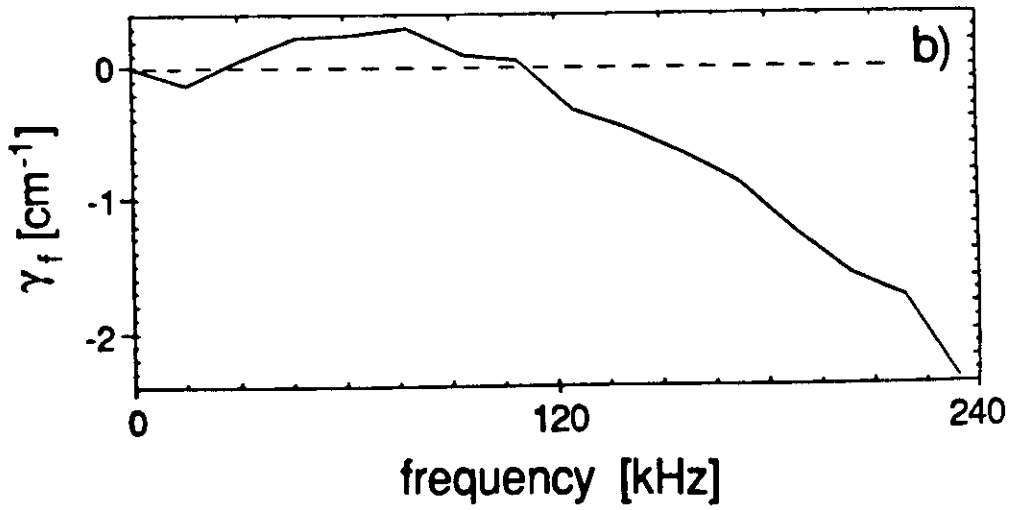

1.5 THEORETICAL MODELS

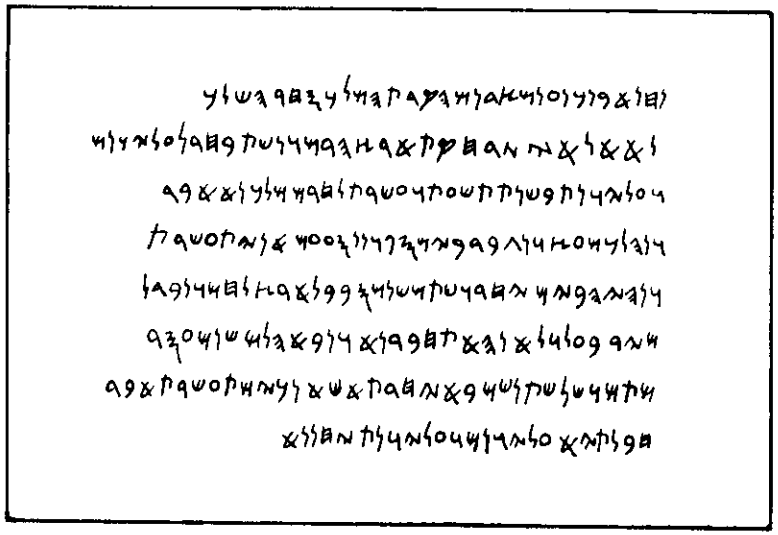

Paraiba Inscription

This tracing of Ladislau Neto's copy of the purported Phoenician inscription was discovered in the 1960's in a scrapbook belonging to Wilberforce Eames, director of the New York Public Library at the end of the last century

ELECTROSTATIC TURBULENCE IN TOKAMAKS

Contents:

2.1 THE PLASMA EDGE

a) Turbulence microscopic description

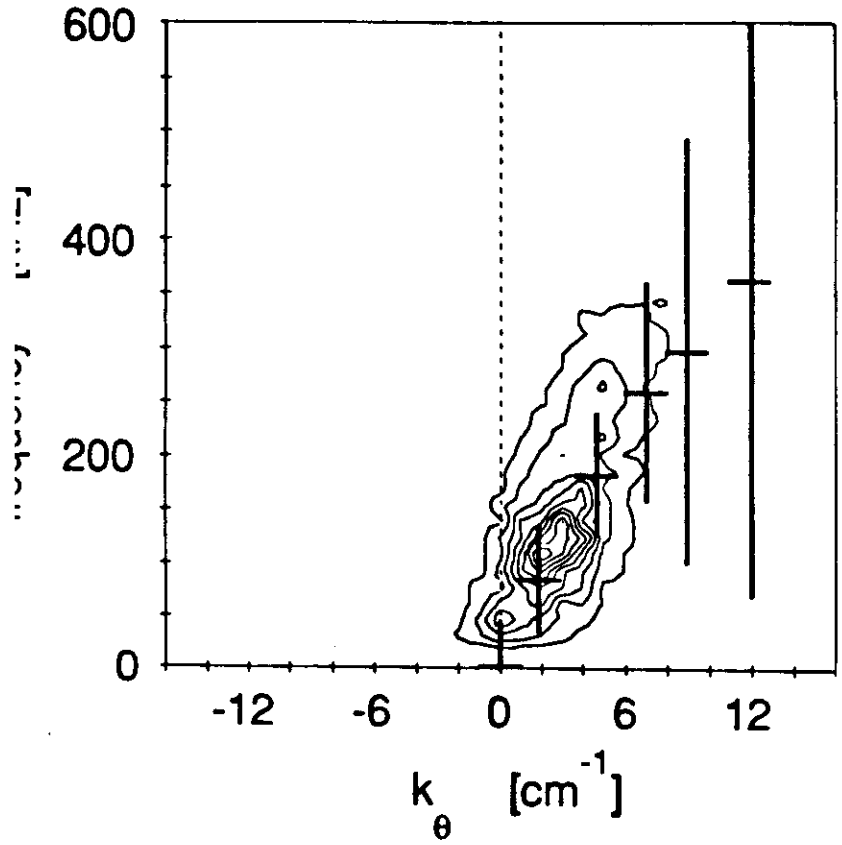

The $S(k_\theta,\omega)$ spectrum at r = 0.255m in TEXT, from Langmuir probes (contours) and FIR scattering (bars indicate FWHM).

$\Delta\omega/\overline{\omega} \approx \Delta k_\theta/\overline{k_\theta} \approx 1$ ($k_\theta\rho_s \approx .1$) demonstrates turbulent nature.

$v_{ph} \approx 3\times10^3 ms^{-1} = v_{de} - E_r/B_\phi$.

$k_\parallel \approx 10/(qR)$, and a mean $\overline{k_r} = 0$. The anisotropy of the turbulence is expressed by the half width $\sigma(k)$ of the $S(k_r,k_\theta)$ spectrum: $\sigma(k_r)/\sigma(k_\theta) \approx 2$, and $\sigma(k_\parallel) \approx k_\parallel$.

The radial dependence of fluctuating parameters

Note $\tilde{\phi}/(k_bT_e) \neq \tilde{n}/n$

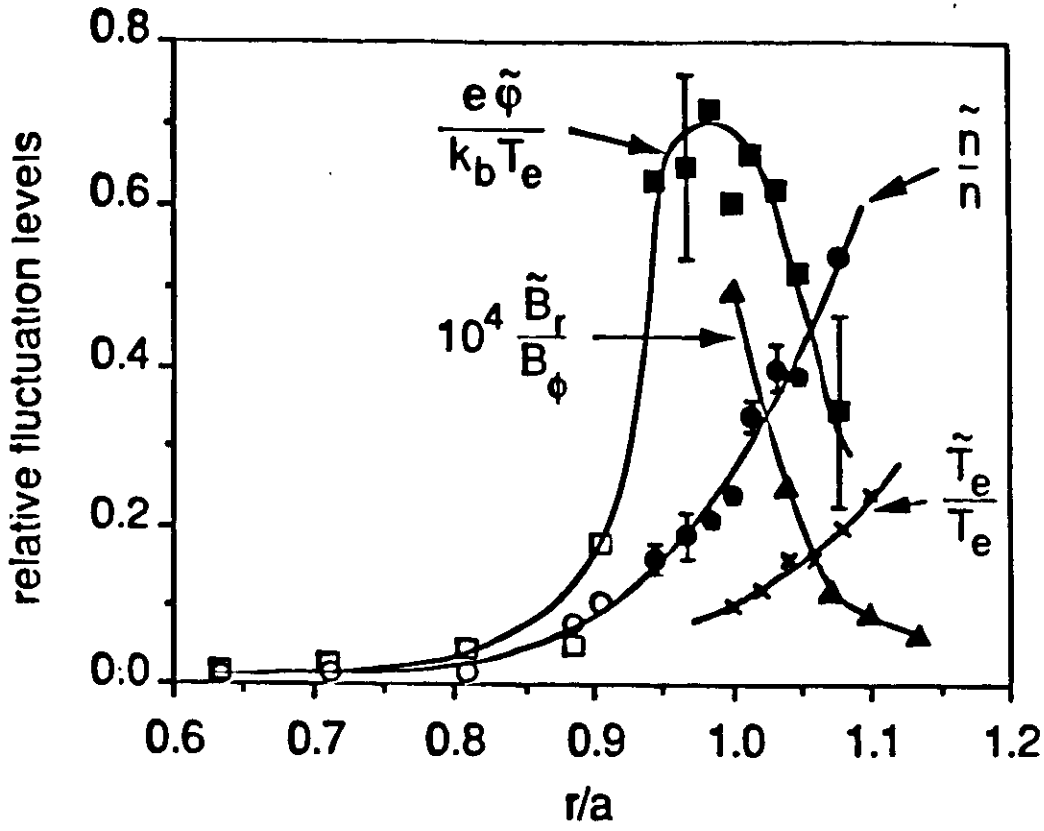

The spatial profiles near the limiter of $\tilde{n}/n$, $\tilde{\phi}/(k_bT_e)$, $\tilde{T}_e/T_e$ and $\tilde{b}_r/B_\phi$ measured with probes in TEXT (B_ϕ = 2T, I_p = 200kA, $\overline{n_e} = 3\times10^{19}m^{-3}$, H^+).

b) Particle fluxes

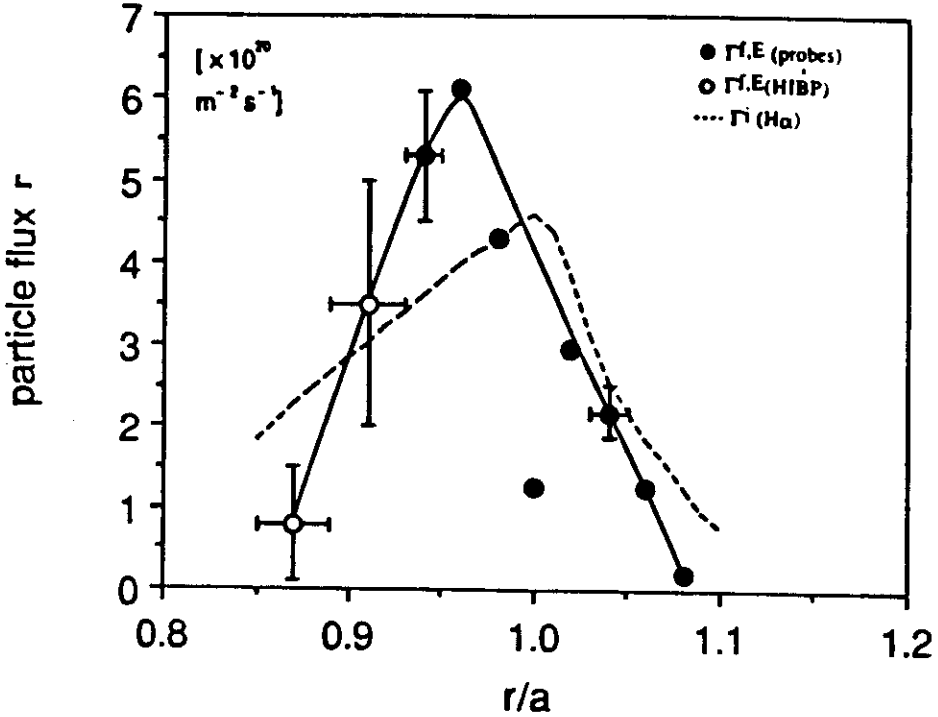

A comparison of working particle fluxes in TEXT (B_ϕ = 2T, I_p = 200kA, $\overline{n_e}$ = $3x10^{19}m^{-3}$, H^+), the total Γ^i (from H_α) and $\Gamma^{f,E}$ driven by electrostatic turbulence. $\Gamma^{f,E}$ is measured with Langmuir probes (solid line, solid points) and the HIBP (open points).

The approximate agreement between $\Gamma^{f,E}$ and Γ^i demonstrates that the measured turbulent fluxes account for an important part, if not all, of the total particle fluxes in the edge.

The agreement is found for a variety of B_ϕ, I_p and $\overline{n_e}$.

Biased limiter results on TEXT show a correlation between reducing E_r (i.e. more negative than the usual value), decreasing Γ^i, (improving τ_p and impurity confinement), and decreasing $\Gamma^{f,E}$.

c) Energy fluxes

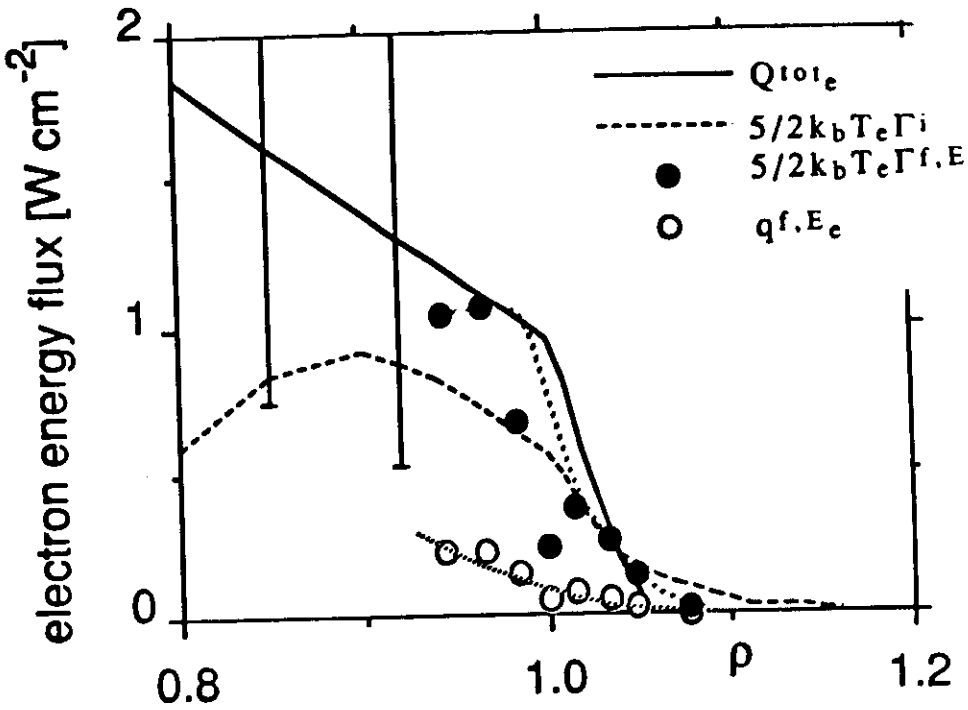

A comparison of power balance and fluctuation driven electron energy fluxes in TEXT. Shown are the total (i.e. power balance) conducted and convected electron energy flux Q^{tot}_e, the total convected electron energy flux $5/2k_bT_e\Gamma^i$, the electrostatic fluctuation driven convected electron energy flux $5/2k_bT_e\Gamma^{f,E}$, and the electrostatic fluctuation driven conducted electron heat flux $q^{f,E}_e$. The total conducted electron energy flux q^{tot}_e is the difference between Q^{tot}_e and $5/2k_bT_e\Gamma^i$ (B_ϕ = 2T, I_p = 200kA, $\overline{n_e}$ = $3x10^{19}m^{-3}$, H^+).

For $\rho > 1$, assuming poloidal and toroidal symmetry, >50% of Q^{tot}_e is accounted for by convection ($5/2\ k_bT_e\Gamma^i$), and this convected energy flux is explained within the error bars by the measured electrostatic fluctuation driven convected energy flux ($5/2.k_bT_e\Gamma^{f,E}$).

The total conducted energy flux $q^{tot}_e = Q^{tot}_e - 5/2\ k_bT_e\Gamma^i$ is approximately equal to the electrostatic fluctuation driven conducted energy flux $q^{f,E}_e$.

The measured magnetic fluctuations provide for a very small conducted power loss: $q^{f,b}_e < 1x10^{-3}Q^{tot}_e$.

d) Theoretical models

	Exp.	collisional ∇n-models (DRIFT WAVE)	∇η-models (RIPPLING)
$\frac{\tilde{n}}{n}$	10 – 50%	≅ $\frac{\rho_s}{L_n}$ or $\frac{1}{k_\theta L_n}$ ≅ 1 – 20% ✓	≅ $T_e^{-1/2} n^{1/2} B_T^{-1/2} \eta$ ≅ 20% ✓
$\frac{e\tilde{\phi}}{k_b T_e}$	≳ $\frac{\tilde{n}}{n}$	≅ $\frac{\tilde{n}}{n}$ ✗	≳ $\frac{\tilde{n}}{n}$ ✓
$\frac{\tilde{T}_e}{T_e}$	≅ (.3 – .5)$\frac{\tilde{n}}{n}$	$\frac{\tilde{T}_e}{T_e}$ ≅ 0 ✗	≅ .3$\frac{\tilde{n}}{n}\frac{L_n}{L_T}$ ≅ (.2 – .4)$\frac{\tilde{n}}{n}$ ✓ ≅ 5 – 15%
$\alpha_{n\phi}$	.2 – .5π	≅ 0 – π (stable) ✗	can be large (>0) ✓
$\bar{k}_\theta$	(2 – 3)cm^{-1}	(2 – 3)cm^{-1} ✓	≅ m/r ≅ 0.5 cm^{-1} ✗
"m-range"	30-100	30-100 ✓	≤ 20 for signific. power ✗

Neither model can reproduce all of the observed characteristics.

In particular the ∇n model cannot yet predict the non-Boltzmann like behavior ($\tilde{\phi}/(k_b T_e) \neq \tilde{n}/n$), the phase angle $\alpha_{n\phi}$, the radial dependence or the scaling of the fluxes. Experimentally, collisionality seems to be unimportant .

The ∇η model fairs better, failing only in its prediction of the high poloidal mode numbers ($\bar{m} \approx 50$) which are measured. Unless $\bar{m} \approx 5$ is used in the ∇η model, the predicted particle fluxes are too small . There appears to be no difference in the turbulence characteristics as the local current density is varied. Of course, it could be that two different mode types are operative with and without I_p, which happen to have similar characteristics.

TRIESTE AJW/FRC 4/26/89

2.2 The Plasma Interior

a) Fluctuation characteristics

A characterization of the results obtained mostly with the scattering diagnostics in which the density of points is intended to represent the value of $\tilde{n}/n$.

Also shown are the scattered power (P_S) frequency spectra for $k_\perp = 1 mm^{-1}$ at various locations, taken from TEXT.

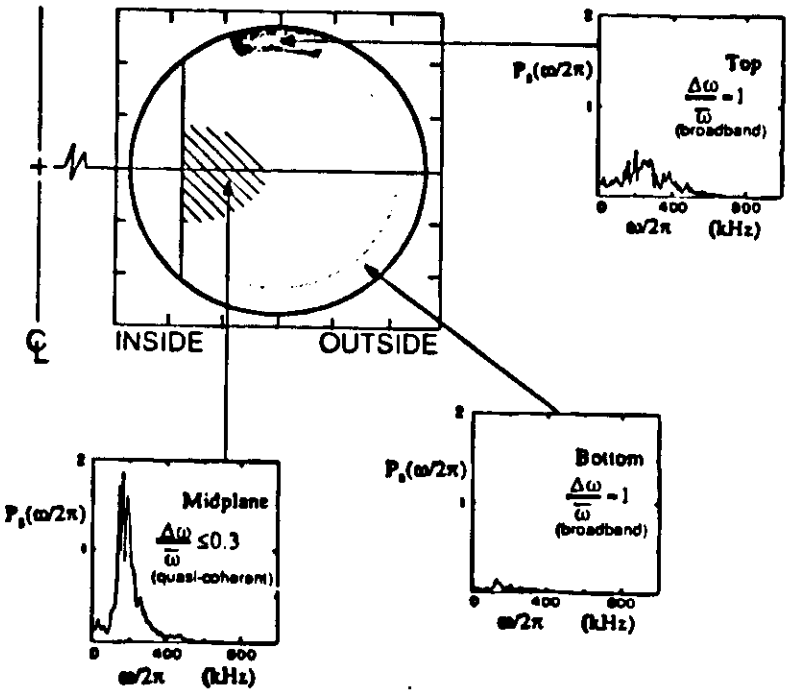

A cartoon of the turbulence from FIR scattering results. The density of points is intended to represent the amplitude of $\tilde{n}/n$. Also shown are the scattered power (P_S) frequency spectra for $k_\perp = 1 mm^{-1}$, with the interaction volume along a vertical chord at R=0.95m (50mm inside of the magnetic axis) above, on and below the midplane (B_ϕ = 2.8T, I_p = 300kA, $\bar{n}_e = 4 \times 10^{19} m^{-3}$, H^+).

BROADBAND TURBULENCE

At the plasma periphery the broadband turbulence ($\Delta\omega/\overline{\omega} \geq 1$, $\Delta k/\overline{k\theta} > 1.5$, both FWHM) is found, independent of sample volume size,with $\widetilde{n}/n \approx 0.3$.

The amplitude generally decreases towards the plasma center where $\widetilde{n}/n \approx 0.01$ (exception: ALCATOR-A), approximately consistent with the mixing length expression $\widetilde{n}/n \approx (\overline{k_r} L_n)^{-1}$ (exception: TFR, PDX).

Most of the power (S) is found at frequencies below 200kHz, and perpendicular wavenumbers $<1/\rho_s$.

The expected drift wave scaling $k\theta\rho_s \sim$ constant is not found; typically $\overline{k\theta}\rho_s$ is between 0.1 and 1.

Where measured $\sigma(k_r) \approx \overline{k\theta}$, and $\overline{k_{||}} << \sigma(k_r), \overline{k\theta}$.

Restricted measurements with an HIBP show within large error bars $\widetilde{n}/n \approx \widetilde{\phi}/(k_b T_e)$: i.e. the Boltzmann relationship may hold in the interior.

The fluctuations propagate in the electron diamagnetic drift direction with a typical phase velocity $v_{ph} \approx 3$ to $5 \times 10^3 ms^{-1}$.

This broadband turbulence is sometimes up-down asymmetric at the plasma edge: such an asymmetry can result from a toroidal asymmetry in the system.

QUASI COHERENT MODES

In TEXT a feature with $\Delta\omega/\overline{\omega} \approx 0.1$, $\Delta k/\overline{k\theta} \approx 0.7$ has been identified at the inner equator, propagating in the electron diamagnetic drift direction with $v_{ph} \approx 1 \times 10^3 ms^{-1}$. This velocity is close to v_{de}.

Scaling studies of this quasi coherent feature show $\overline{k} \alpha B_\phi^{0.7} I_p^{-0.2}$, $\overline{k\theta}\rho_s \approx 0.6$. The scaling of $\widetilde{n}/n$ (αB_ϕ^{1}) is very different from the broadband feature scaling (where $\widetilde{n}/n \alpha B_\phi^{-1}$).

A similar quasi coherent mode has been identified on PDX, right at (within 3 to 5ms) the H mode onset. In this case the feature had $\omega/(2\pi) \approx 40$ to 100kHz, $\Delta\omega/\omega \approx 0.03$, $m \approx 15$ to 20, and $\widetilde{n}/n \approx 1$ to 20%.

ION FEATURE

A third feature, broadband and propagating in the ion drift direction, has also been identified.

The spectral power density in the ion feature (S_i) relative to that in the broadband electron drift feature (S_e) increases with increasing $\overline{n_e}$.

Ignoring complications which arise in the analysis of S_e and S_i from any plasma mass rotation, S_i/S_e increases on TEXT from 0.08 to 0.5 as $\overline{n_e}$ is increased from 2 to $8 \times 10^{19} m^{-3}$, with $B_\phi = 2.8T$ and $I_p = 400kA$.

No such feature has been found in He discharges, and its strength is reduced when the plasma is fueled with hydrogen pellets, rather than molecular hydrogen and recycled hydrogen ions. An interpretation in terms of the ion temperature gradient mode is discussed later.

With the above picture it is clear that spatial asymmetries are important, and unlikely that any single model will explain all the details of the interior fluctuations.

It is also clear that trying to correlate fluctuation levels and confinement properties will be difficult.

It is unlikely that we will ever be able to determine identically the individual fluctuation driven energy fluxes, as we can at the edge. Instead, we will have to rely on theoretical models to interpret limited data. This should not necessarily be regarded as a restriction, because an understanding of the turbulence implies that we have a model to explain it.

The radial dependence of $\tilde{n}/n$ for the broadband feature

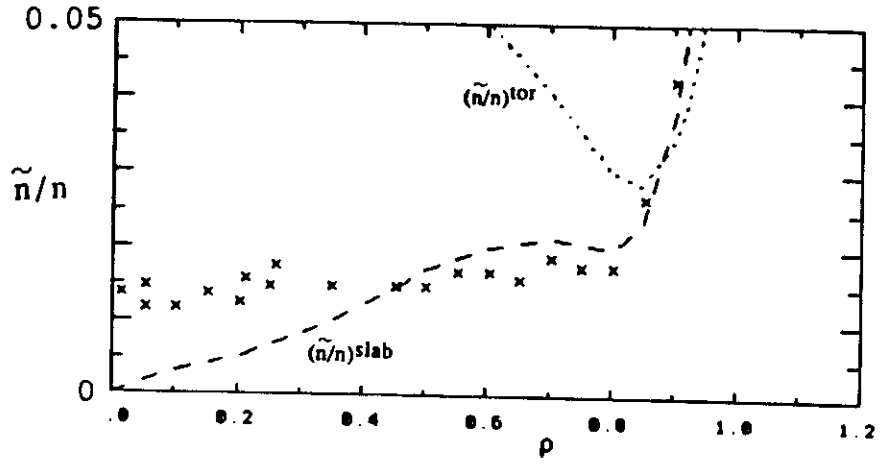

The spatial variation of $\tilde{n}/n$ from TEXT (B_ϕ = 2T, I_p = 200kA, $\bar{n_e}$ = 2 to $3\times10^{19}m^{-3}$, H^+), shown as crosses (HIBP). Also shown are the predictions of two mixing length estimates, $(\tilde{n}/n)^{tor}$ and $(\tilde{n}/n)^{slab}$. Both electron feature $\tilde{n}/n$ and $k\theta$ ($\bar{k\theta}\rho_s$ = 0.1) are interpreted assuming no ion feature is present.

Slab geometry ($k_r \approx \rho_s^{-1}(L_n/L_s)^{1/2}$):$(\tilde{n}/n)^{slab} = \rho_s L_n^{-3/2} L_s^{1/2} \approx 3\rho_s/L_n$

Toroidal geometry ($k_r \approx k\theta \hat{s}$): $(\tilde{n}/n)^{tor} \approx 1/(k\theta\, \hat{s}\, L_n)$.

$L_n = -n(dn/dr)^{-1}$, $L_s = Rq/\hat{s}$, and $\hat{s} = r/q.\partial q/\partial r$.

Insufficient information exists at all radii to use measured values of $k\theta$ (which affects $(\tilde{n}/n)^{tor}$), so we have invoked the drift wave scaling $\overline{k\theta}\rho_s \approx c$, with c an experimentally determined constant.

Both at $\rho \approx 1$ (Langmuir probes, HIBP, FIR) and at $\rho \approx 0.5$ (HIBP) we measure $c \approx 0.1$.

The better representation is then given by $(\tilde{n}/n)^{slab}$.

However, if $c \approx 0.4$, both $(\tilde{n}/n)^{tor}$ and $(\tilde{n}/n)^{slab}$ fit the experimental results equally well: values of $c \approx 1$ are found on other machines.

Neither model predicts the measured $(\tilde{n}/n) \approx 1\%$ at the plasma axis.

The presence of counter-propagating fluctuations in the HIBP data will lead to an underestimate of the relevant value of $\overline{k\theta}$ and an overestimate of the relevant value of $\tilde{n}/n$. Counter-propagating fluctuations have been seen (the ion feature, but are measured and expected to be at a low level at low $\overline{n_e}$ (the reason for analyzing a comparatively low density discharge). Using the measured plasma parameters for the particular discharge predicts no ion feature (because $\eta_i = d\ln(T_i)/d\ln(n_i) < 1.5$, the critical value for instability onset). However, the experimental uncertainties allow theoretical values of $(\tilde{n}/n)\eta_i \approx 1\%$

b) Particle fluxes

The radial variation of the working particle flux Γ^i, $\Gamma^{f,E}$ and Γ^{dw} (DTE and universal mode, slab geometry for the quasi linear turbulence regime).

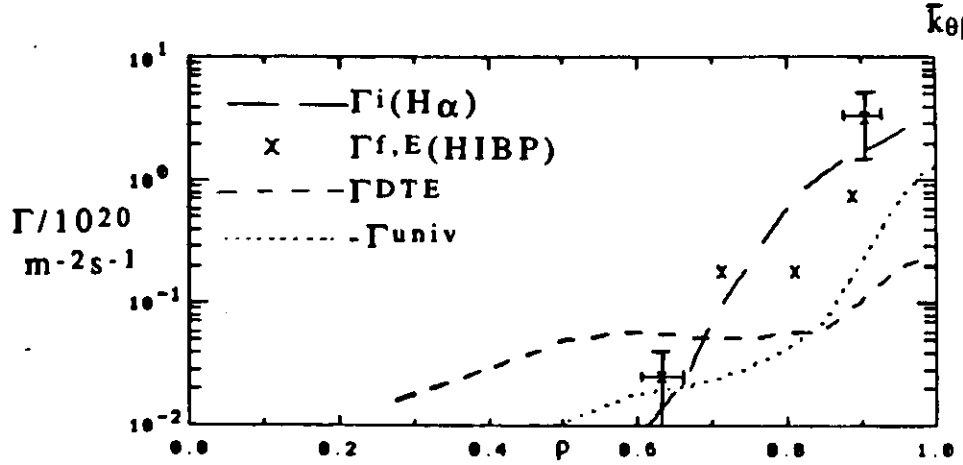

The spatial variation of various working particle fluxes on TEXT (B_ϕ = 2T, I_p = 200kA, $\overline{n_e} = 3\times10^{19}m^{-3}$, H^+).

DTE mode is unstable and the universal mode is marginally unstable for the measured $k\theta$ values. However, stable modes could be excited at higher k and the energy cascade down to the measured k.

Both Γ^{DTE} and Γ^{univ} are shown regardless of their regimes of applicability. Γ^{DTE} is applicable for $0.2 < \rho < 0.7$ and Γ^{univ} is applicable for $0.7 < \rho < 0.95$. Γ^{DTE} is outward (>0), and Γ^{DTE} is inward (<0).

Γ^i is explained by the measured $\Gamma^{f,E}$, Γ^{DTE} does not predict the correct spatial dependence, and Γ^{univ} predicts an inward instead of an outward flux. However, various limitations on each of the fluxes Γ^i, $\Gamma^{f,E}$ and Γ^{dw} must be considered.

LIMITATIONS

Γ^i: H_α measurement limited by the inversion procedure. Using a computed source from a neutral transport code, we get a much higher value of Γ^i.

$\Gamma^{f,E}$: Counter propagating turbulence will reduce $\overline{k\theta}$, $\gamma_{n\phi}$, and $\alpha_{n\phi}$. Therefore $\Gamma^{f,E}$(HIBP) could be incorrect (the results were obtained in a discharge in which the ion feature was at a very low level). Upper limit: use the measured $\tilde{n}/n$, but assume $\alpha_{n\phi} = 90^0$, $\gamma = 1$, and $\overline{k\theta\rho_s} = 0.4$.

Γ^{dw} : This is affected by $\overline{k\theta\rho_s}$. To obtain an upper limit we use the measured $\tilde{n}/n$ and a value $\overline{k\theta\rho_s} = 0.4$.

LIMITATIONS

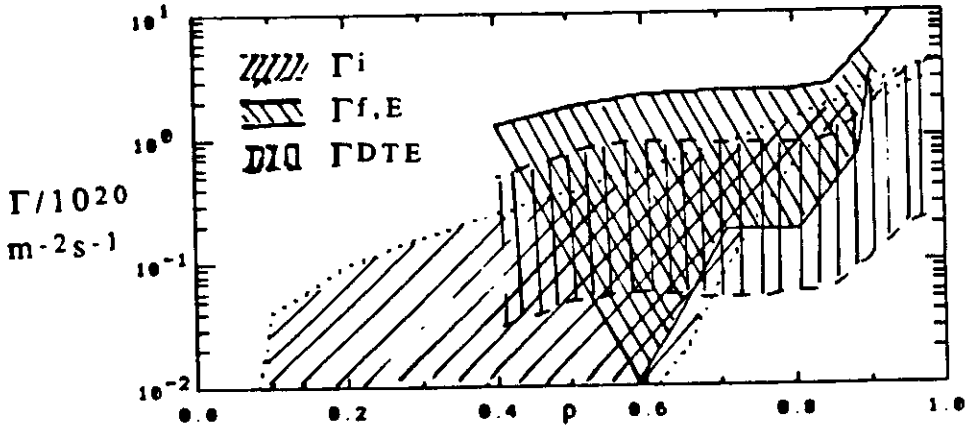

Limits to the spatial variations of various working particle fluxes on TEXT (B_ϕ = 2T, I_p = 200kA, $\overline{n_e} = 3\times10^{19}m^{-3}$, H^+). 1) Γ^ilower = $\Gamma^i(H_\alpha)$ = 0; 2) Γ^iupper from a neutral particle transport code calculation (ANTIC); 3) $\Gamma^{f,E}$lower = $\Gamma^{f,E}$(HIBP); 4) $\Gamma^{f,E}$upper from $\Gamma^{f,E}$(HIBP) but assuming optimum phase angle and coherence with $\overline{k\theta\rho_s}$ = 0.4; 5) Γ^{DTE}lower using the measured $\tilde{n}/n$ and assuming $\overline{k\theta\rho_s}$ = 0.1; and 6) Γ^{DTE}upper using the measured $\tilde{n}/n$ and assuming $\overline{k\theta\rho_s}$ = 0.4.

With these limitations to the fluxes, it is possible that $\Gamma^i = \Gamma^{f,E} = \Gamma^{DTE}$; Γ^{univ} is still inward (<0). We must reduce these uncertainties by factors >10 before we can show discrepancies between the various fluxes.

DIFFUSION AND CONVECTION

D(ρ) and v^i(ρ): $v^i > 0$ is outward.

Split the theoretical drift wave fluxes into a D ($\alpha\nabla n$) and a v (everything else), with $k\theta\rho_s = 0.1$ and 0.4.

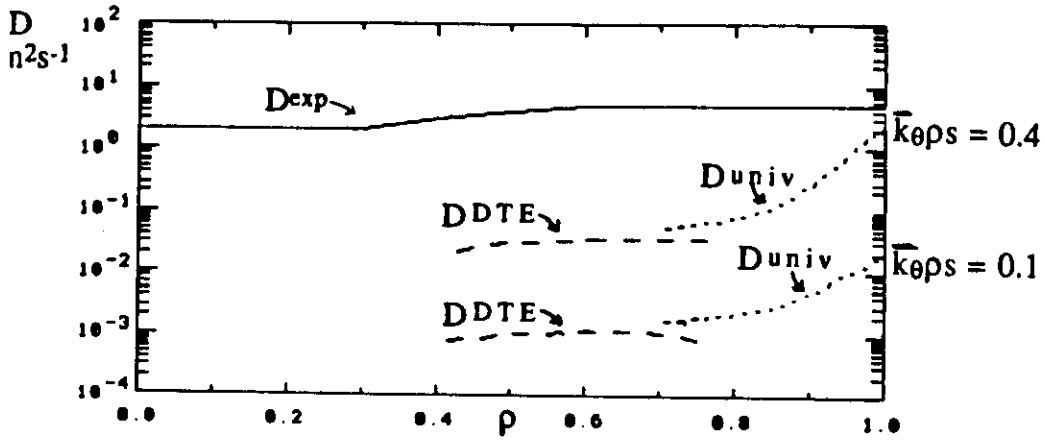

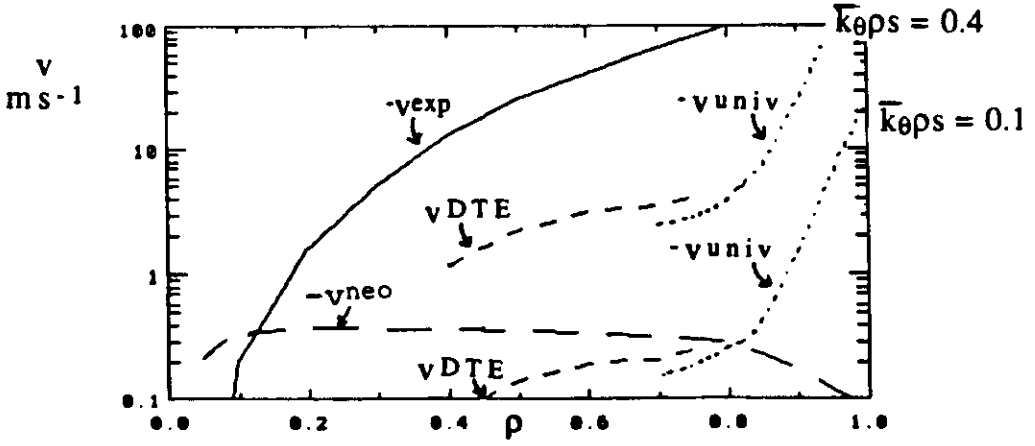

DIFFUSION AND CONVECTION

D(ρ) and v^i(ρ): $v^i > 0$ is outward.

Split the theoretical drift wave fluxes into a D ($\alpha\nabla n$) and a v (everything else), with $k\theta\rho_s = 0.1$ and 0.4.

The spatial variation of working particle diffusion coefficient D (Figure a) and convection velocity v (Figure b) on TEXT (B_ϕ = 2T, I_p = 200kA, $n_e = 3\times10^{19}m^{-3}$, H^+). Shown are the experimental values D^{exp} and v^{exp} deduced from oscillating gas puff experiments, together with the predictions of two drift wave turbulence models, dissipative trapped electron (D^{DTE}, v^{DTE}) and universal (D^{univ}, v^{univ}). Both models are for quasi linear turbulence in slab geometry, and evaluated using HIBP measured $\tilde{n}/n$. Results are shown assuming both $\bar{k}\theta\rho_s = 0.1$ (as measured) and $\bar{k}\theta\rho_s = 0.4$. Also shown is the neoclassical pinch velocity v^{neo}. Note the signs of v.

The DTE model predicts an outward convection velocity, with negligible diffusion (because $(\bar{k\theta}\rho_s)^2 << 1$; however, the turbulent $\Delta\omega$ affects this term).

The universal mode predicts an inward convection velocity, but is inapplicable in the region $\rho < 0.7$. The ion pressure gradient inward flux is not predicted to be induced in this discharge (because $\eta_i < 1.5$), but the uncertainties are large.

While the uncertainties in the experimental v^i are large, the neoclassical inward pinch v^{nc}, also shown, is generally too small.

c) Heat fluxes-electron

Generally no correlation between $\tilde{n}/n$ and energy confinement time τ_E is found for Ohmic heated discharges.

Spatial asymmetries are important, and unlikely that any single model will explain all the details of the interior fluctuations.

Trying to correlate fluctuation levels and confinement properties will be difficult. It is unlikely that we will ever be able to determine identically the individual fluctuation driven energy fluxes, as we can at the edge. **Instead, we will have to rely on theoretical models to interpret limited data.** One should not necessarily expect to find a simple correlation between a line of sight measurement of $\tilde{n}/n$ and a measure of confinement, for example the heat flux q, the energy confinement time τ_E, or the thermal diffusivity χ_e. This is so for at least three reasons.

1) a line of sight (subscript los) value $(\tilde{n}/n)_{los}$ is dominated by edge phenomena, where $\tilde{n}/n$ is largest, and changes in $(\tilde{n}/n)_{los}$ may have nothing to do with changes in internal fluctuation levels.

2) asymmetries change with differing plasma condition, and these can affect $(\tilde{n}/n)_{los}$ even though a local value of $\tilde{n}/n$ has not changed.

3) even if a local measurement of $\tilde{n}/n$ is available, no theory predicts simply that χ_e = constant x $(\tilde{n}/n)^a$: other variables appear in the 'constant'. For example, in quasi linear drift wave theory a = 2 and the 'constant' α T_e, amongst many other parameters. In strong turbulence theories a = 1, and it has been suggested that a = 0 for stochastic regimes.

Notwithstanding these arguments, the results from TFR discussed later clearly show that τ_E^{-1} α $(\tilde{n}/n)2$.

TRIESTE AJW/FRC 4/26/89

An example

q^{tot}_e, q^{DTE}_e and q^{univ}_e (in their regions of applicability)

a) $k\theta\rho_s = 0.1$ b) $k\theta\rho_s = 0.4$.

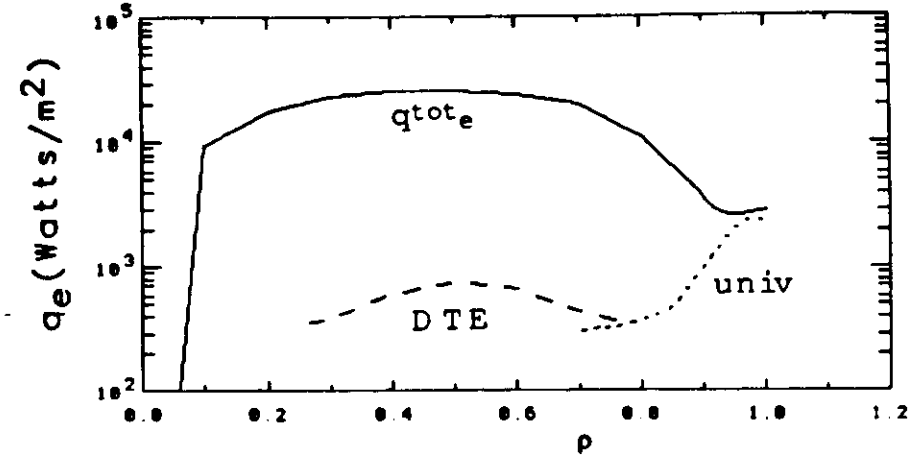

a) The radial dependence of the experimental conducted electron heat flux q^{tot}_e in TEXT (B_ϕ = 2T, I_p = 200kA, $\bar{n}_e = 2\times10^{19}m^{-3}$, H^+), and the prediction of drift wave turbulence q^{dw}_e using experimentally measured turbulence characteristics (HIBP measured S(k,ω) with both electron feature $\tilde{n}/n$ and $k\theta$ ($\bar{k\theta\rho_s}$ = 0.1) interpreted assuming no ion feature). Results are shown for the dissipative trapped electron (DTE, broken line) and universal (univ, dotted line) modes.

$\bar{k\theta\rho s} = 0.4$

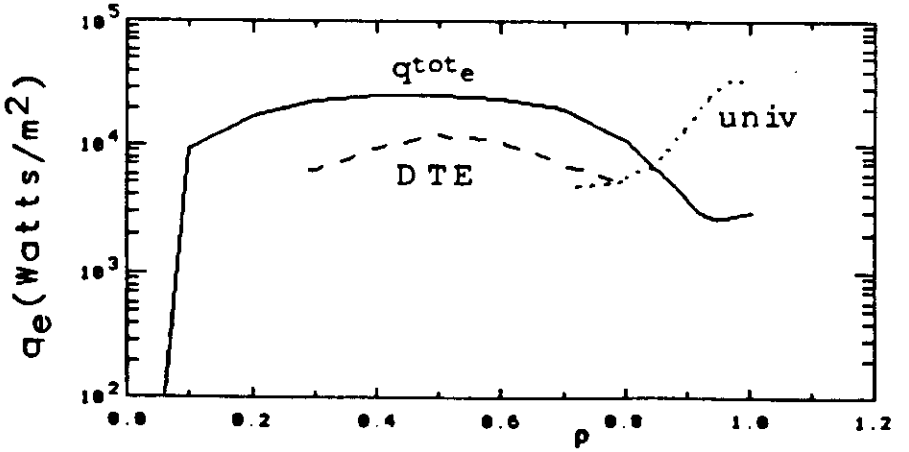

b) As for figure a), but assuming that $\bar{k\theta\rho_s}$ = 0.4, rather than the measured 0.1.

With $k\theta\rho_s = 0.1$ both the DTE and universal modes show $q^{dw}_e < q^{tot}_e$.

Predictive computer codes which claim good agreement with experiment in the DTE regime, i.e. they suggest $q^{dw}_e \approx q^{tot}_e$. The difference between the experiment and the modeling is primarily that the measured $\overline{k\theta\rho_s} \approx 0.1$, rather than ≈ 0.5 as is assumed in the codes. Using $\overline{k\theta\rho_s} \approx 0.4$ leads to approximate agreement between q^{dw}_e and q^{tot}_e in TEXT.

We must understand the role of any ion feature (affecting S).

Other turbulence models should be tested in a similar manner.

ADDITIONAL HEATING in TFR

a) ion cyclotron heating b) neutral beam heating.

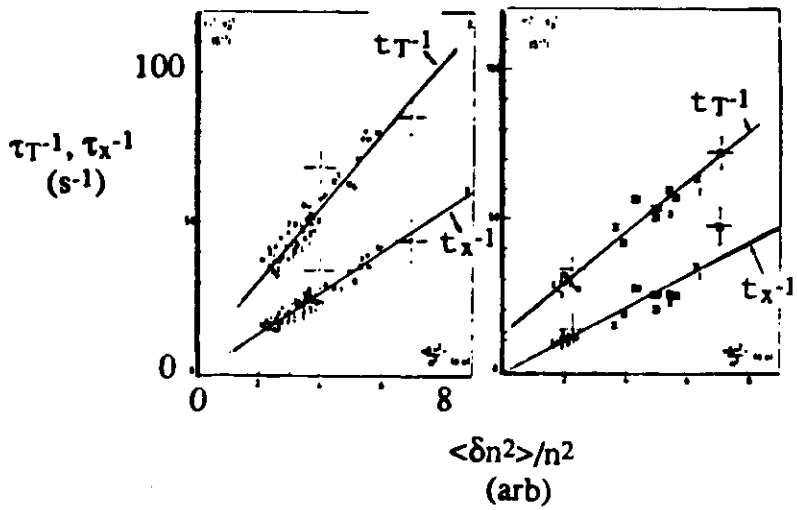

The correlation between energy confinement time and density fluctuation level obtained on TFR Figure a) concerns ion cyclotron heating, and Figure b) concerns neutral beam heating. Small graphic symbols refer to Ohmic heating, and large graphic symbols to additional heating. $<\delta n^2/n^2>$ is the line of sight frequency integrated relative fluctuation level at one k. τ_T is the electron energy confinement time (conduction and convection), and τ_x the confinement time with the losses from sawteeth removed.

Small graphic symbols: Ohmic heating, large graphic symbols: additional heating. $<\delta n^2/\overline{n^2}>$ is the line of sight frequency integrated fluctuation level at one k, normalized to the line of sight average density. τ_T is the electron energy confinement time (conduction and convection), and τ_x the confinement time with the losses from sawteeth removed.

Increased electron conduction losses are associated with increased line of sight values of $(\tilde{n}/n)^2$.

OTHER IDEAS

$\chi_e^{HP} > \chi_e^{PB}$ might be explained by an increased fluctuation driven q_e resulting from plasma parameter or gradient changes. Enhancements in $\tilde{n}/n$ coincident with sawtooth collapse are seen on TFR, ASDEX, TEXTOR and TEXT. In TFR and TEXTOR a high frequency burst is found, at a time corresponding to the collapse and poloidal expansion of the hot core. The cell of enhanced turbulence is localized within $r_{q=1}$, and extends poloidally about 120^0 to 180^0. The sawtooth radial heat pulse is poloidally asymmetric, in line with the high frequency cell.

Both intrinsic (i.e plasma generated) and extrinsic (i.e externally imposed) magnetic islands are found to affect $\tilde{n}/n$ significantly, perhaps demonstrating a sensitivity to local plasma parameters such as L_n.

Alternative models to explain q_e invoke magnetic fluctuations, and measurements to support or disprove this point of view are described later.

d) Heat fluxes-ion: an example from ALCATOR-C.

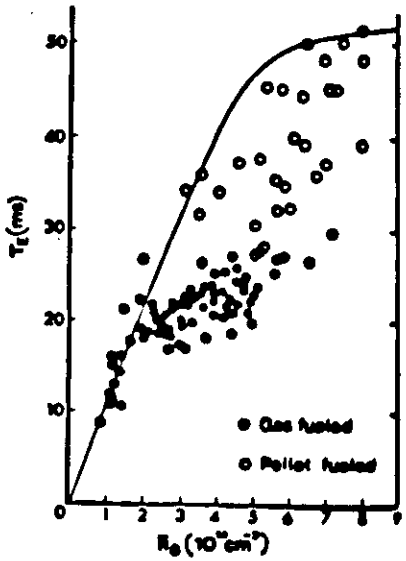

The global energy confinement time τ_E as a function of density $\bar{n}_e$, from ALCATOR-A (B_ϕ = 10T, I_p = 750kA, H^+). Results with both edge fueling (solid circles) and frozen pellet fueling (open circles) are shown. The solid line is the energy confinement time expected using neo-ALCATOR scaling for χ_e and 1xChang-Hinton (neoclassical) for χ_i

As the density is increased by gas puffing in ohmic heated discharges a saturation in global energy confinement time τ_E is found.

Coincident with the saturation of τ_E is an increasing collisional coupling between the electrons and ions, so that the ion channel becomes more important in determining the total energy confinement. If the ions behaved neoclassically the saturation would occur at higher $\bar{n}_e$; the ion losses are anomalous.

A mechanism to explain the anomaly is the ion pressure gradient, or η_i, mode.

If the η_i mode is responsible for the anomalous χ_i, then peaking the density profile should reduce η_i, stabilize the η_i mode, reduce χ_e, and increase τ_E. With pellet fueling and the ensuing peaked density profiles, τ_E does indeed increase. However, the cessation of sawteeth with pellet fueling has also been proposed as an explanation for this improvement.

EVIDENCE FOR THE η_i MODE?

If the η_i mode is responsible for the anomalous χ_i, then an ion feature should be observed in the fluctuation spectrum. Figure shows a comparison of the S(ω) spectra for three discharges on TEXT, a) at low density with gas puff fueling, b) at high density with gas puff fueling, and c) at high density with pellet fueling.

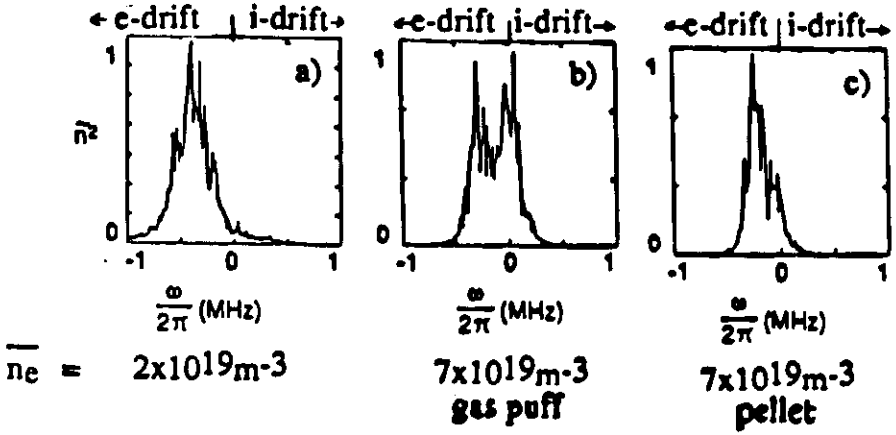

The power spectrum S(ω) in arbitrary units for $k_\perp = 9cm^{-1}$, obtained with FIR scattering on TEXT: a) low density gas puff ($B_\phi = 2.8T$, $I_p = 250kA$, $\overline{n_e} = 3x10^{19}m^{-3}$, H^+) b) high density gas puff ($B_\phi = 2.8T$, $I_p = 250kA$, $\overline{n_e} = 6x10^{19}m^{-3}$, H^+), and c) high density pellet fueled ($B_\phi = 2.8T$, $I_p = 250kA$, $\overline{n_e} = 6x10^{19}m^{-3}$, H^+). Negative frequencies correspond to propagation in the electron diamagnetic drift direction

An ion feature (S_i) is seen, whose strength increases as $\overline{n_e}$ increases with gas puff fueling. Unfortunately the TEXT results do not show a clear increase in τ_E when this feature is reduced.

2.3 SUMMARY

There is at least one exception to almost every statement made.

The edge plasma

The turbulence is broadband ($\Delta\omega/\overline{\omega}$, $\Delta k_\theta/\overline{k_\theta} > 1$) with frequency $\overline{\omega}/2\pi \approx$ 100kHz, a mean poloidal wave number $\overline{k_\theta} \approx 200m^{-1}$, a mean radial wave number $\overline{k_r} \approx 0$, and parallel wave number $\overline{k_\parallel} \approx 1m^{-1}$. The ratio of half widths σ(k) of the $S(k_r,k_\theta)$ spectrum is $\sigma(k_r)/\sigma(k_\theta) \approx 2$, and $\sigma(k_\parallel) \approx \overline{k_\parallel}$. Typical fluctuation levels are $\tilde{n}/n \approx 0.2$, $\tilde{\phi}/(k_bT_e) \approx 0.3$, $\tilde{T}_e/T_e < 0.1$, and $\tilde{b}_r/B_\phi \approx 1x10^{-5}$.

Where measured the electrostatic turbulence is responsible for a large part, if not all, of the edge particle fluxes; Γ^i and $\Gamma^{f,E}$ agree in both amplitude and scaling with parameters (B_ϕ, I_p, $\overline{n_e}$, impurity content, E_r).

The energy fluxes are less well accounted for by the electrostatic fluctuations, but the error bars are large. In ohmic heated low β plasmas the measured $\tilde{b}$, interpreted using a quasi linear formula, is too small to contribute to the thermal losses.

The edge turbulence is well characterized, but no completely satisfactory model has been found which predicts all the measured features. The least problematic is the resistivity gradient model, which fails only in its prediction of the m numbers. An up-down asymmetry has been isolated, perhaps a result of toroidal asymmetries, for example the limiter or the discrete toroidal field coils.

The plasma confinement region

Fluctuation measurements are presently restricted to $\tilde{n}$, $\tilde{\phi}$ and their correlations. Three distinct features are observed.

1) the broadband turbulence, with characteristics similar to those at the edge. Both $\tilde{n}/n$ and $\tilde{\phi}/(k_b T_e)$ decrease towards the plasma center, and $\bar{k}\rho_s \approx 0.1$ to 1 (but with caveats on the interpretation of $\bar{k}$ because of the possible presence of an ion feature). The fluctuations propagate in the electron diamagnetic drift direction. This feature is often attributed to drift wave turbulence and invoked to explain experimental q_e.

2) quasi-coherent modes has been identified at the high toroidal field side of the plasma.

3) at high densities, a broadband feature propagating in the ion drift direction is found, which has been associated with the ion pressure gradient driven , or η_i, mode. This mode is used to explain χ_i which in turn is invoked to explain the saturation of τ_E at high densities.

Clearly the spatial dependence of the fluctuations is complicated. This fact, and the theoretically expected complicated relationship between $\tilde{n}/n$ and a flux or transport coefficient, means that we should not necessarily expect to find a simple relationship between a line of sight or single point measurement of $\tilde{n}/n$ and a plasma transport coefficient or a flux.

The characteristics of the observed fluctuations have been compared with the predictions of the models suggested to explain them. We have also compared the measured plasma transport properties with those predicted to result from the modes, using where possible measured turbulence properties. We find:

1) $(\tilde{n}/n)^{exp} \approx (\tilde{n}/n)^{slab}$ on a log-log scale. Individual machines shows significant departures. The problems of data interpretation in the presence of counter propagating turbulence are important in this comparison.

2) $\bar{k}\rho_s \neq$ constant: the problems associated with a counter propagating turbulence are important in this comparison. There is evidence for the expected B_ϕ dependence of $\bar{k}_\theta$,but little evidence for the T_e or mass dependence.

3) The slab collisional, universal and dissipative trapped electron drift wave modes are respectively stable, marginally unstable and unstable at the measured k_θ values.

4) The broadband feature, interpreted as quasi linear drift wave turbulence, does not explain the usual description of interior particle transport. However, limitations in the measurements of both total and fluctuation driven particle flux should be recognized.

5) The broadband feature, interpreted as quasi linear drift wave turbulence, does not explain the measured interior electron heat flux. This is in contrast to predictive code calculations: the difference lies in the assumed and measured values of $\tilde{n}/n$ and $\bar{k}_\theta$. The experimental values are uncertain because of the problems associated with data interpretation in the presence of counter propagating turbulence. While the choice of working ion affects q^{tot}_e, it does not affect q^{dw}_e for the model considered. It is important to understand and correctly interpret the effects of any ion feature. More detailed measurements of $\bar{k}$ are required.

6) The measured ion temperatures are approximately predicted using the sum of the neoclassical and pressure gradient driven ion thermal fluxes. The measured ion feature suggests the presence of the ion pressure gradient driven mode. The characteristics of the ion feature should be further investigated (e.g. the scalings of $\tilde{n}/n$ and $\bar{k}$).

MAGNETIC TURBULENCE IN TOKAMAKS

Contents:

3.1 Coherent MHD activity

a) m/n = 1/1 and sawteeth

An example of typical soft x-ray signals obtained from TFTR.

a) simple sawtooth oscillations: the large m/n = 1/1 precursor oscillations are seen clearly on the channel viewing r = 10cm.

b) small sawteeth are similar, but the m/n = 1/1 activity is different, there being a large successor oscillation to the crash.

c) compound sawteeth; each compound sawtooth consists of a subordinate relaxation followed by a large (up to 20% in central T_e) main relaxation.

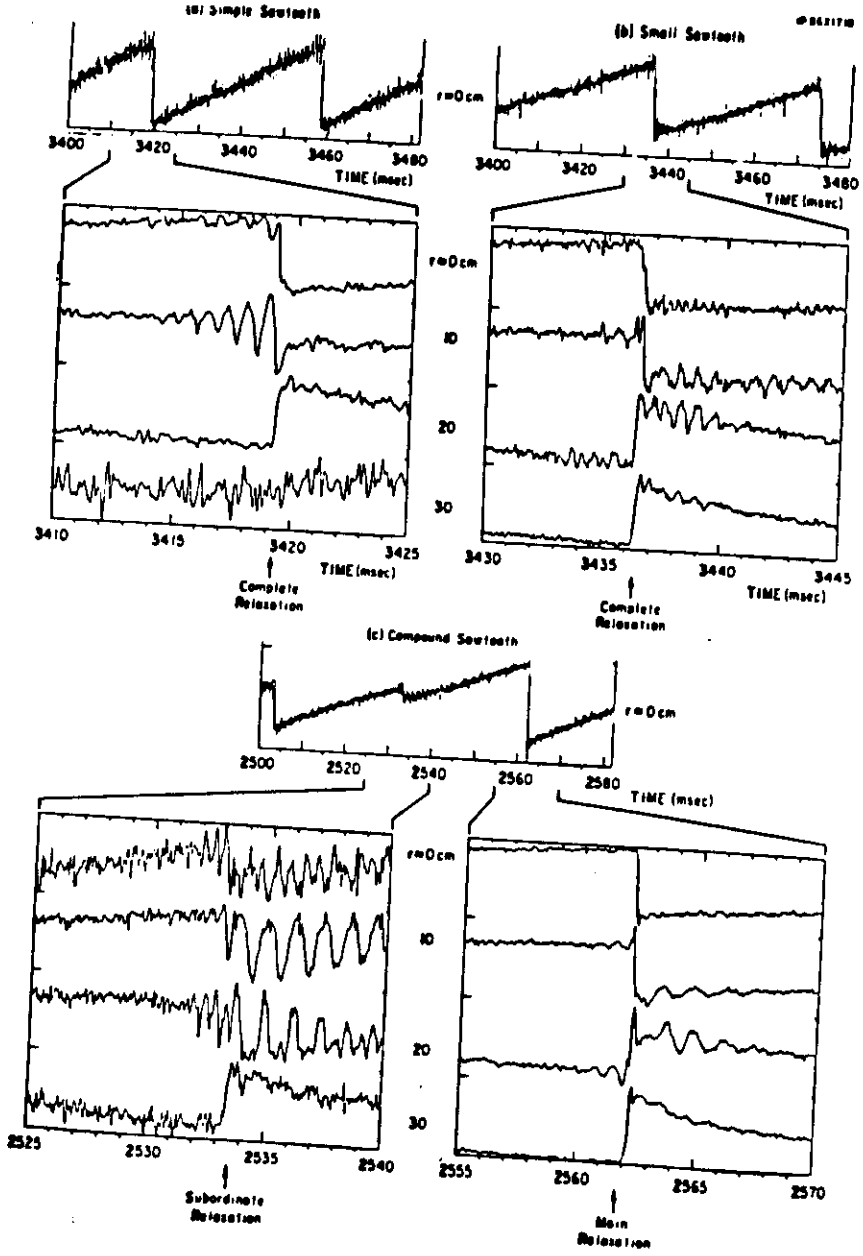

Soft X-ray signals from TFTR, illustrating three different types of sawtooth activity. a) Simple sawtooth with an m/n = 1/1 precursor, b) small sawtooth with a continuous m/n = 1/1 signal, and c) compound sawtooth. For each example the signals displayed with expanded timebase illustrate the m/n = 1/1 activity

52a

m/n = 2/1,3/1

Early experiments on TOSCA revealed the presence of the expected tearing mode activity, together with a high frequency component.

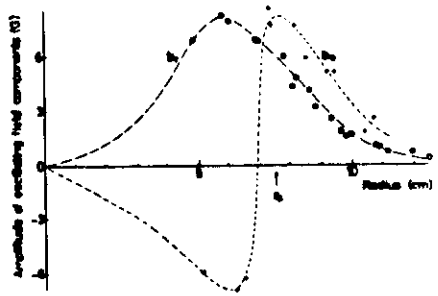

Radial distribution of oscillating radial and poloidal field components. The radius at which q = 3 is indicated by r_s.

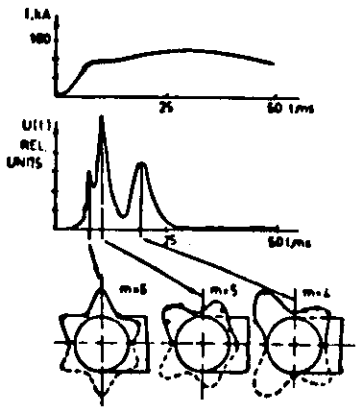

Coherent MHD modes observed during the plasma current rise phase of T-3

COHERENT MAGNETIC FLUCTUATIONS AND TRANSPORT

Mode m/n	Effects	Understanding
1/1	sawteeth?	q profile information needed Stochastic or reconnection?
2/1	degrades confinement major disruption	islands enhance χ_e
3/2	degrades confinement	islands enhance χ_e
4/3, 5/4	small effects on confinement	observed with high beta
m = 10-15	edge transport?	observed close to edge changes with L-H transition

HIGH BETA MHD ACTIVITY

The observed spectrum of MHD fluctuations at high beta is clearly dominated by the n = 1 mode when the q = 1 surface is in the plasma: this mode does not by itself significantly affect τ_E. The m/n = 1/1 mode drives other n = 1 modes through toroidal coupling and $n \geq 1$ modes through nonlinear coupling.

3.2 INCOHERENT MODES

a) General characteristics, and
b) relationship to electrostatic fluctuations

Here we are concerned with the breakup of magnetic surfaces from overlapping magnetic islands. Electron heat transport follows, with any particle transport coming from the associated density fluctuations driven with the magnetic fluctuations. If this mechanism is responsible for transport, then $\chi_e \propto \eta(m_i \beta/m_e)^{1/2} (\alpha/s)^{3/2}$, with $\alpha = -2Rp'/B_\phi^2$, and $s = rq'/q$.

Typically $\tilde{b}/B_\phi \approx 10^{-4}$ to 10^{-5} is measured, with the amplitude increasing towards smaller plasma radius. Generally no correlation between the (edge) electrostatic and magnetic fluctuations is found except when the electrostatic measurements ($\tilde{\phi}$ or $\tilde{n}$) are made inside the main plasma, at $r < a$. In the case of ohmically heated TOSCA, the measured $\tilde{b}$ is consistent with being a result of $\tilde{n}$ rather than $\tilde{n}$ being a result of $\tilde{b}$.

As in the case of density fluctuations, diametrically opposite conclusions have been reached. For example,

Ohmically heated TOSCA and additionally heated (L mode) TFR: no correlation between $\tilde{b}$ and confinement properties was found.

Ohmic heated TCA and Tokapole , and additionally heated JET and ISX-B : a clear correlation between increasing $\tilde{b}$ and decreasing energy confinement is found.

TRIESTE AJW/FRC 4/26/89

c) Correlation with tokamak confinement

Results from JET, in which at high values of β_p large increases in $\tilde{b}$ have been seen (see also TOSCA).

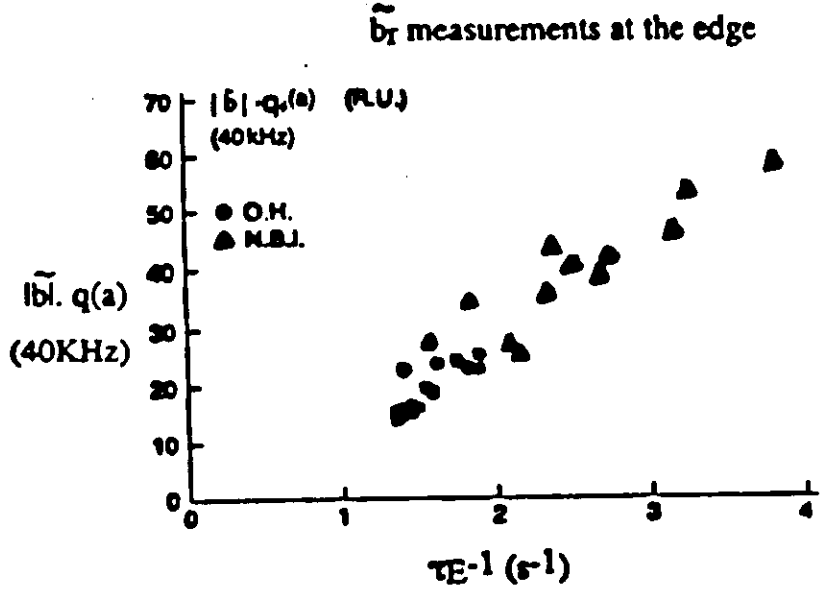

The relationship between $\tilde{b}_{\theta q}(a)$ and energy confinement time τ_E obtained on JET for ohmic and neutral beam injected (NBI) plasmas.

Results from DIII-D demonstrate that the broadband magnetic turbulence is correlated with the quality of confinement. The amplitude changes abruptly at the transition between various modes of confinement: ohmically heated, L mode, H mode, and during ELM's (edge localized modes). The fluctuation amplitude is largest where the separatrix intersects the divertor plates, which is interpreted as evidence for the existence of line tied image currents in the scrape off later, beyond the separatrix. However, there is a problem with interpreting these transitions as being solely due to changes in $\tilde{b}$. The different modes (L and H) refer to particle as well as electron energy confinement, and magnetic stochasticity is not generally expected to influence particle transport.

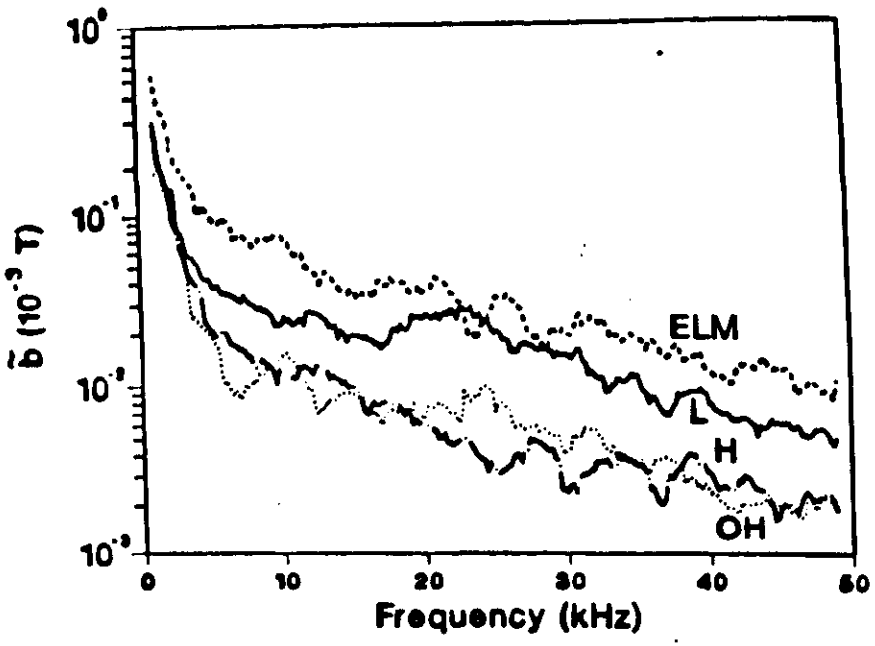

16) The frequency spectra of the magnetic fluctuations in DIII-D at the outer divertor hit spot for ohmical heated (OH), low confinement (L), high confinement (H) and during periods with edge localized modes present (ELM) [201].

PROBLEMS

TFTR and TCA show that the amplitude level is extremely sensitive to local edge boundary conditions.

FT show sensitivity to plasma position.

These result may partially explain why different machines get different results for the correlation between τ_E and $\tilde{b}$.

Quantitative calculations of the effects of the measured $\tilde{b}$ are difficult. First it must be decided if the (usually) externally measured $\tilde{b}$ represents edge or interior phenomena. Different conclusions have been reached concerning this point. The measured $\tilde{b}$ must be extrapolated to the value of $\tilde{b}$ at the resonance surfaces, a check made to ensure island overlap has occurred, and then a formula chosen to infer local electron heat transport. To explain χ_e using the quasi-linear expression $\tilde{b}_r/B_\phi$ must decrease from $\approx 1 \times 10^{-3}$ at the periphery to $\approx 1 \times 10^{-4}$ near the center, whereas limited results show the opposite radial dependence. Unless strong turbulence formulae are invoked (c.f. JET), it is usually true that the inferred $\tilde{b}$ is too small using existing models and formulae, except at high β values . Externally generated magnetic stochasticity produces an electron heat flux consistent with the quasi-linear result.

OTHER OBSERVATIONS

Other (than coil) diagnostics have been used to infer internal magnetic structure.

On ALCATOR-A, anomalies in the soft X-ray spectrum were interpreted in terms of $\tilde{b}$ and this was considered to explain the internal electron heat fluxes.

The ratio of runaway to thermal energy confinement has also been used to infer internal magnetic structure. Runaway confinement is improved over thermal confinement because of the phase averaging over magnetic perturbations when the drift surfaces are displaced from the magnetic surfaces. On ASDEX a correlation between degraded τE and increasing internal $\tilde{b}$ (deduced from runaway electron confinement) is claimed.

Other evidence that magnetic stochasticity is playing a role in transport comes from measurements of plasma potential Φ: at low densities $\Phi(a) > 0$ and this has been interpreted as being caused by electron loss to a limiter across stochastic magnetic fields. Externally imposed stochastic layers clearly increase the edge plasma potential Φ and electric field E_r.

3.3 EXTRINSIC MAGNETIC PERTURBATIONS

a) Magnetic surfaces, islands and stochasticity

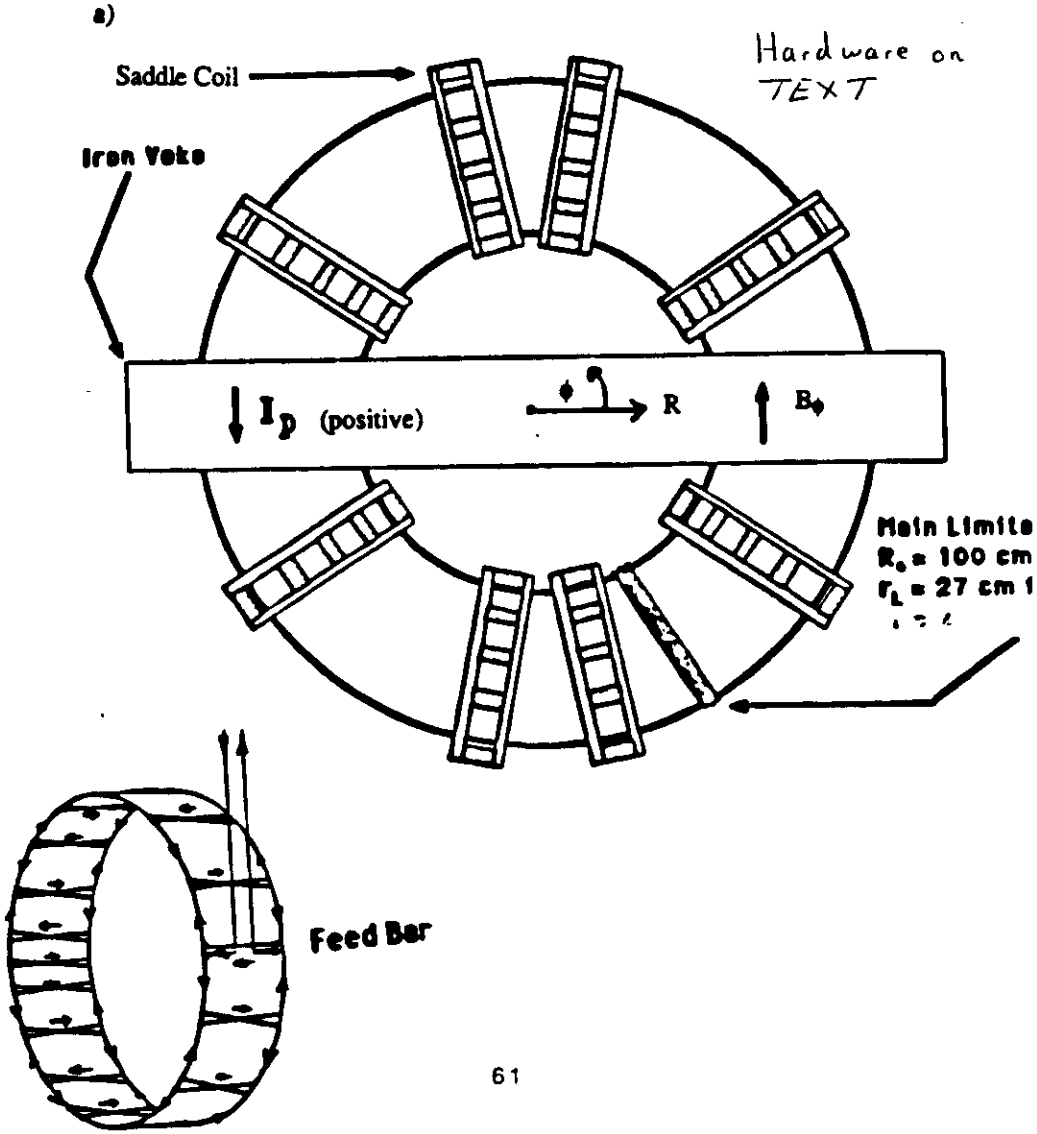

Examples of Poincaré Plots

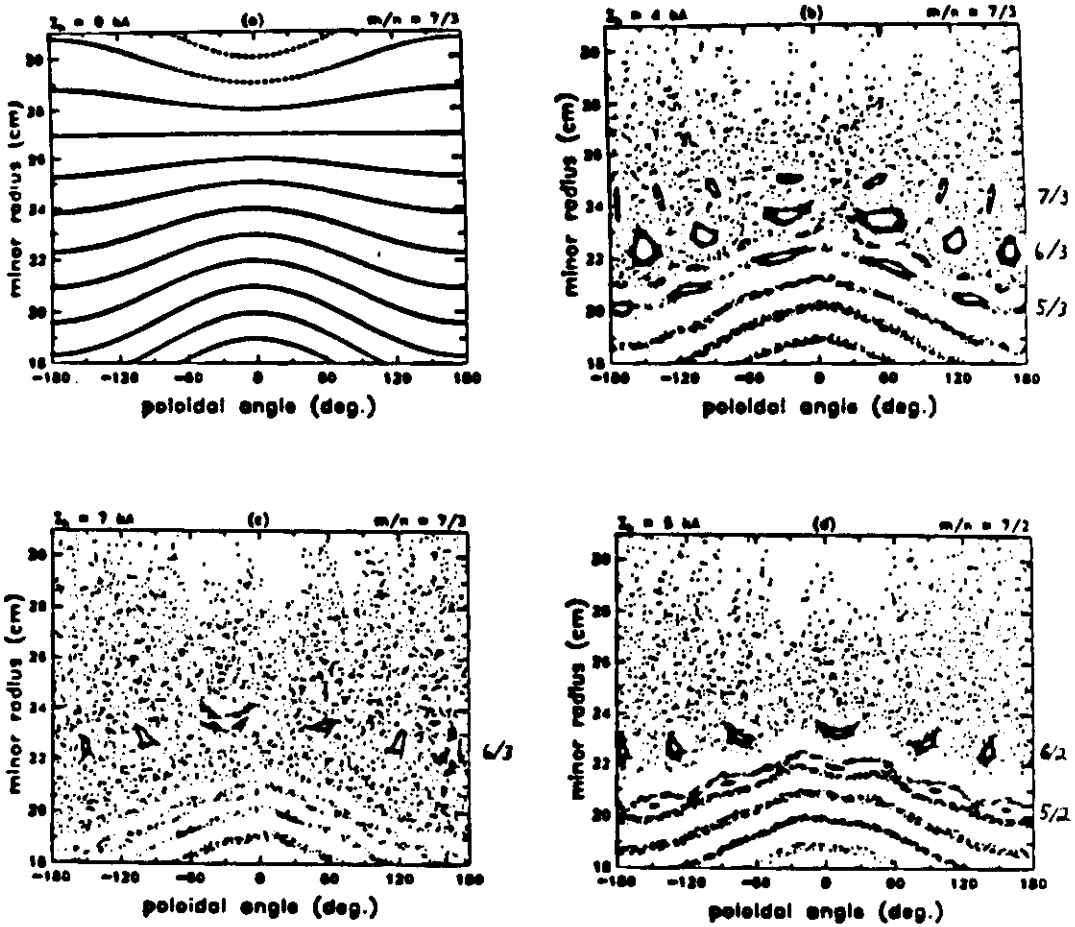

61a)

The Magnetic Diffusion Coefficient

$$D_m = \lim_{L \to \infty} \frac{1}{2} \frac{d(\Delta r)^2}{dL}$$

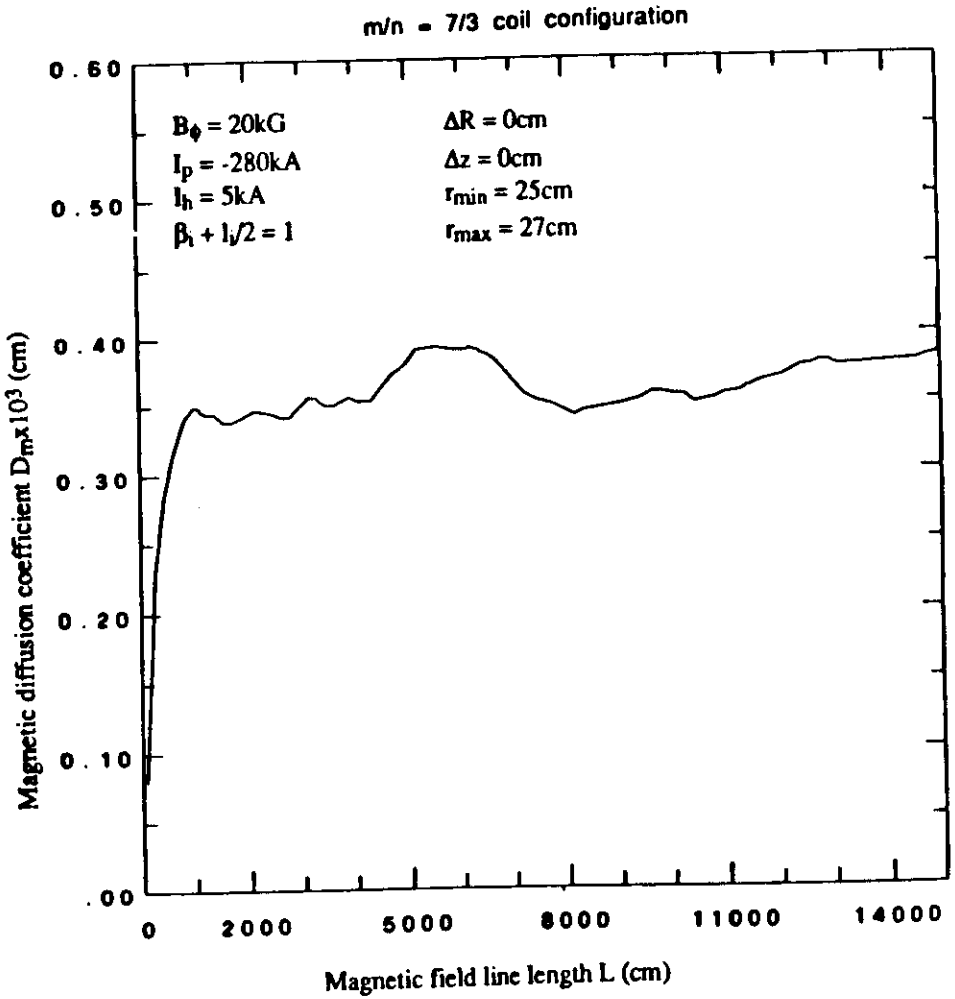

m/n = 7/3 coil configuration

61b

b) The motivation

Stochastic layers => edge parameter control (increase edge diffusion => cool edge, Fewer impurities and increased impurity out-flux)

Islands used for "Intra-island pump limiters" - channel heat and particles directly into an aperture in a limiter For particle control

c) General effects

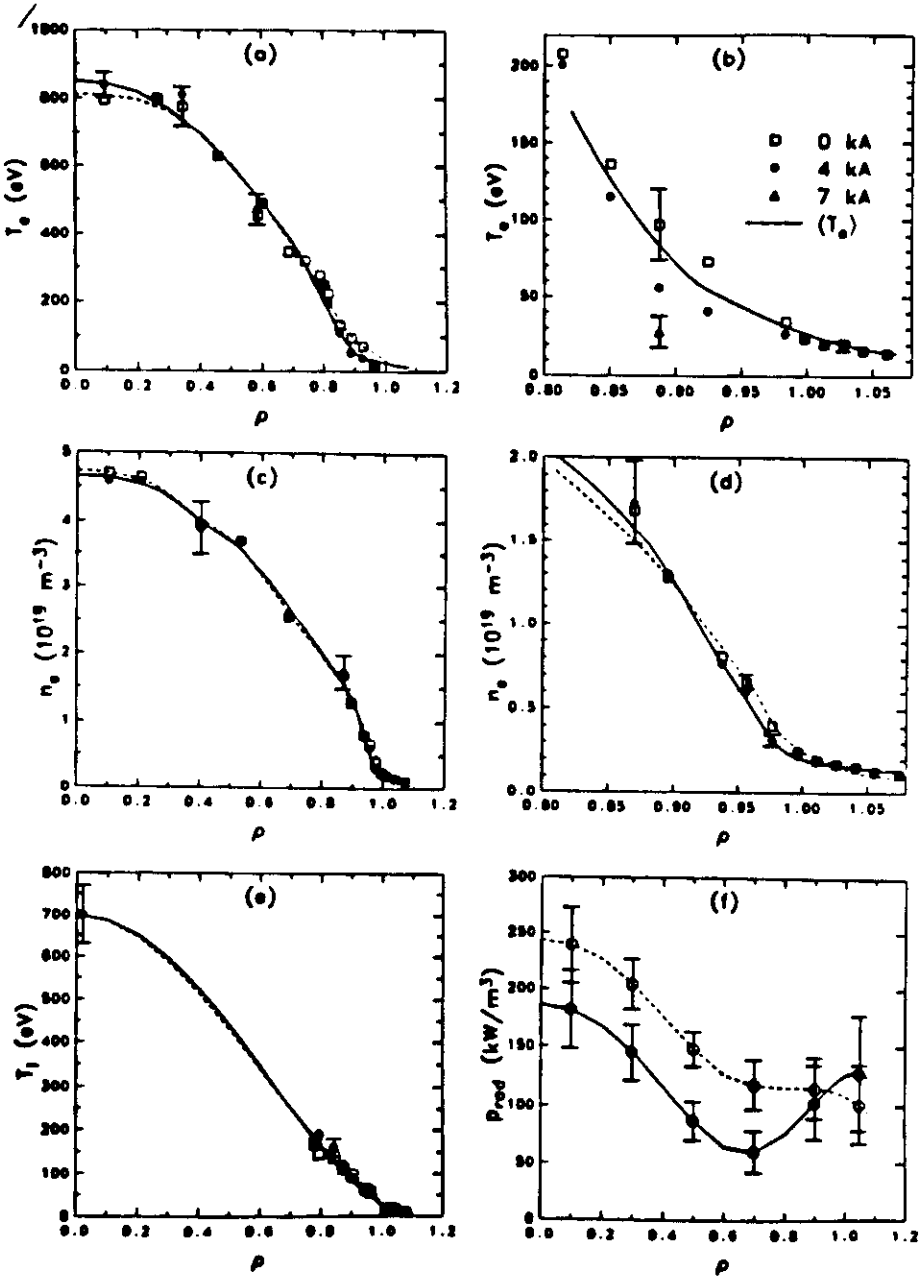

TEST PARTICLE SIMULATION

The analytic theories for test particle motion in a stochastic field usually assume strongly overlapping islands: this is not true for our experiment.

Therefore calculate particle motion in the perturbed fields.

Include parallel motion along field lines, with Coulomb collisions.

Include the intrinsic electrostatic turbulence as a random walk, displacing particles a distance ρ_c (in a time τ_c) away from their initial unperturbed trajectory. ($D_{exp} = \rho^2/2\tau_{cexp}$, with τ_c the experimental coherence time ~ $1/\Delta\omega$).

The experimental $T_e(r)$ and $n_e(r)$ specify e.g. v_{th}, D_{ll}, $\lambda_{Coulomb}$.

Calculate particle diffusion for electrons or ions from the time taken for a distribution of particles to cross a specified radial distance.

Equate D_{ion} with D^i, $D_{electron}$ with χ_e.

Self consistent effects are not included (E_r, poloidal asymmetries).

Real sources and sinks are included.

TRIESTE AJW/FRC 4/26/89

d) Particle confinement

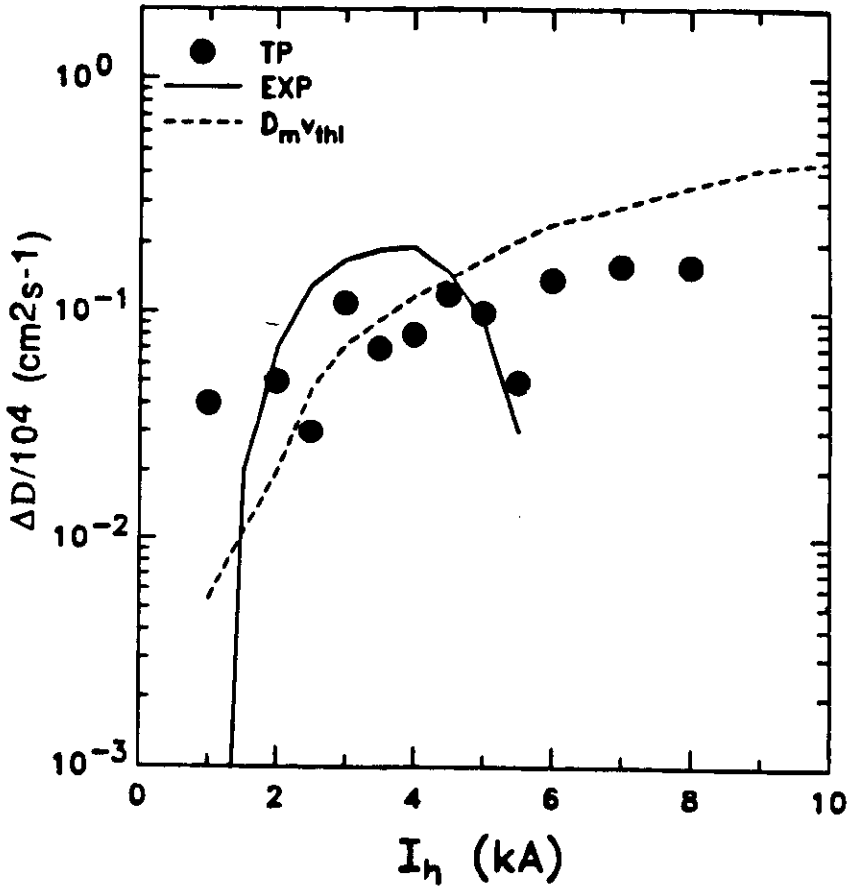

- Experiment shows a clear peak in $D_\perp$ for $I_h \approx 4$kA: neither the test particle model or the simple expression predicts this.

4 Possible explanation for the peak in $D_\perp$

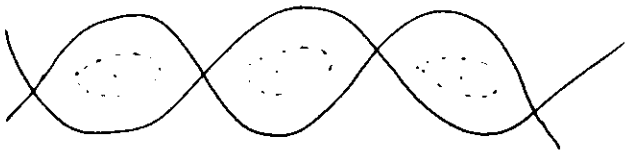

$E_h = 4kA \equiv$ island width maximum. 3 ways round an island; $\perp$ // or poloidal rotation ($E_r \times B_\phi$)

$$\tau_{ExB} = 1/(k_y V_{ExB}) \qquad \tau_{v\|} = \frac{2Ls}{\Delta x}\,\frac{1}{k_y V_i} \qquad \tau_{turb} = \frac{\Delta x\, Ln}{D}$$

$$\left(L_s = \frac{R\,q^2}{r\,q'}\right) \qquad \text{With e n } E_r = p_i/L_p,$$

$$\frac{\tau_{ExB}}{\tau_{v\|}} = \frac{\Delta x}{2\rho_i}\,\frac{L_p}{Ls} \cong \frac{1}{3}$$

$$\frac{\tau_{ExB}}{\tau_{turb}} \cong \frac{1}{16\,k_y \Delta x}\,\frac{D}{D_{Bohm}}$$

For m = 7 ($k_y = 0.043\text{cm}^{-1}$), Δx = 1cm,

$$\tau_{turb} > \tau_{ExB} \text{ unless } D \lesssim D_{Bohm}$$

e) Energy transport

$$\chi_e^{RR} = D_m D_\parallel / L_H$$

$$\chi_e^{KP} = (D_m/J_\perp)\,(D_\parallel D_m)^{1/2}$$

$$\left.\begin{aligned}\chi_e^{F} &= \chi_{e\parallel}\left(\frac{b_r}{B_\phi}\right)^2 \\ \chi_e^{c} &= \langle D_m \rangle v_{the}\end{aligned}\right\} \text{ Simple formulae fit the results}$$

Ranges of validity: valid; valid within a factor of 2

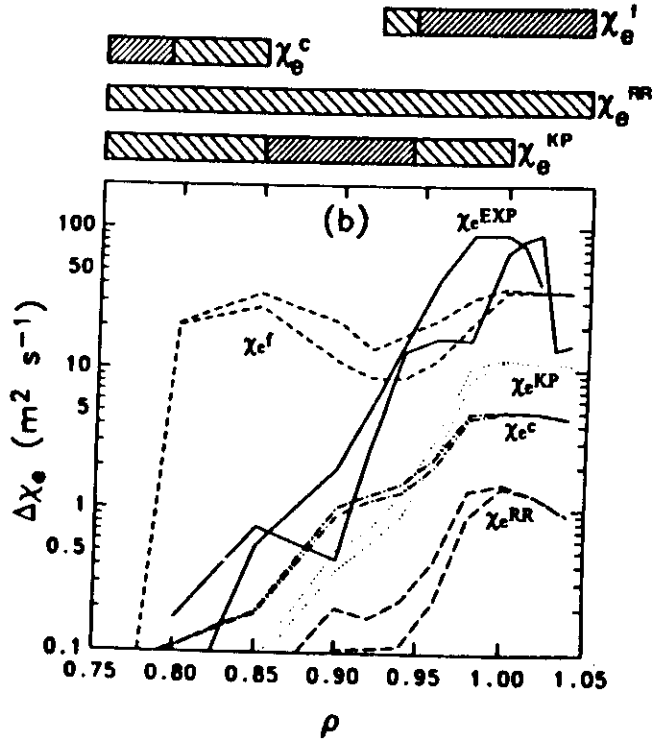

Dependence of $\Delta\chi_e$ on I_h ($\propto (b_r/B_\phi)$)

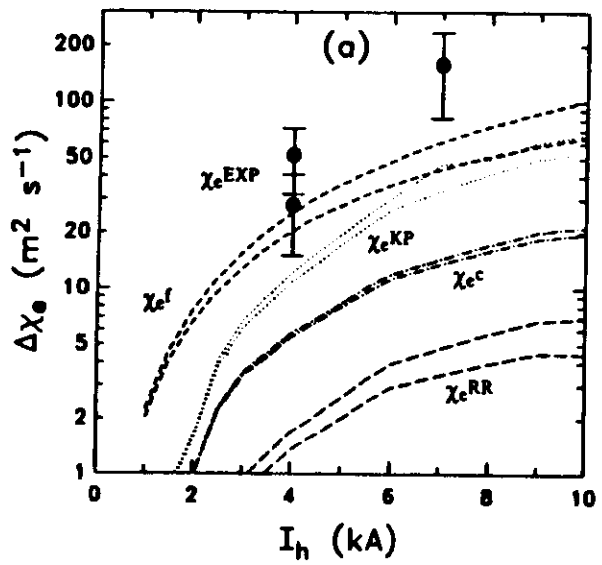

* at the edge, $\chi_e \simeq \chi_e^{I}$; scaling $\simeq$ OK
(don't expect simple $\left(\frac{b_r}{B_\phi}\right)^2 \propto I_h^2$, because $\frac{b_r}{B_\phi}$ affects $\chi_{e\parallel}$)

SUMMARY

To draw any conclusions concerning the role of $\tilde{b}$ in determining interior confinement is impossible, except perhaps to say that there is generally little correlation between τ_E and $\tilde{b}$ in Ohmic discharges (exception, TCA, TOKAPOLE), and more of a correlation as β_p is increased. As in the case of density fluctuations, spatial asymmetries, the choice of turbulence model, the location of the $\tilde{b}$ signal and other variable plasma parameters might account for the many different observations. Clearly localized, internal measurements of $\tilde{b}$ in a tokamak are required if further progress is desired.

Externally imposed perturbing fields are comparatively well understood. In particular:

$\chi_e \sim v_{the}\langle D_m\rangle$ for a collisionless plasma

$\chi_e \sim \chi_{e\parallel}(b_r/B_\phi)^2$ for a collisional plasma

Self consistent E_r may play an important role in determining D^i.